

The optimal tuning, within carbon limits, of thermal mass in naturally ventilated buildings

Salmaan Craig^{a,*}

^a*School of Architecture, McGill University, Montréal, QC, Canada*

Abstract

What proportions should a thermally massive building have? How should the thermal mass be distributed? Should the "massing" change with the choice of material? This paper shows how to optimize the physical proportions of a building so that it synchronizes ambient heat exchanges in a natural feedback cycle. An internal mass is thermally coupled with buoyancy ventilation; the cycle is driven by the daily swing of outdoor temperature. Tripling up functions in this way—so that structural materials can reliably cool and power the ventilation for buildings—could help decarbonize the construction industry and provide an effective strategy for adapting to life-threatening heatwaves. Based on harmonic analysis, the method allows designers to thermally tune the form and mass of a building to meet chosen targets for temperature and ventilation in free-running mode. Once the optimal balance of exchange rates is known, design teams can proportionally vary the building height and ventilation openings against the surface area and thickness of an internal thermal mass. The possible permutations are infinite but parametrically constrained, allowing teams to fairly compare the functional and environmental credentials of different construction materials while they produce and evaluate preliminary options for organizing the exterior form and interior spaces of a building. An example study suggests that thin-shell structures of minimum weight, and even timber buildings, may be optimally tuned to produce ample ventilation and temperature attenuation.

Keywords: Thermal mass, Natural ventilation, Thermal Resilience, Materials design, Life Cycle Analysis, Thermal optimization, Low carbon

1. Background

In the next decade, building design teams may be forced to shrink and simplify the material inventories of their design proposals to meet strict limits on greenhouse gas emissions [1–3]. As well

*Corresponding author.

Email address: salmaan.craig@mcgill.ca (Salmaan Craig)

as using construction materials in smaller quantities and for longer lifetimes, the emphasis will be on finding intelligent ways of organizing, shaping, and upgrading these materials, so that ancillary building products and artificial climate control are less needed, and renovation, reuse, and recycling are more straightforward in later life-stages [4, 5]. The method outlined in this paper is meant to help design teams achieve this kind of material integration—within carbon limits and without sacrificing the physical and spatial qualities of the architecture, or overdetermining its possible uses in an uncertain future.

It may be some time before the industry establishes a consensus on how to accurately account for the carbon-dioxide emissions associated with construction. Efforts are underway to improve the quality of emissions data, make them widely and freely available, and to standardize the accounting and reporting procedures [6–8]. However, as one study recently highlighted [9], the discrepancy between results from different carbon accounting methods can be significant—larger, even, than the savings either method estimates for alternative design schemes. This scale of uncertainty is disabling for decision-makers. It seems to propagate in proportion to the number of components: the more complex the material assembly, the more difficult it is to get an accurate picture of the potential web of ecological upheaval. Reducing the material intensity of buildings could, therefore, result in a double dividend: real reductions in carbon-dioxide emissions, and more reliable predictions of these reductions.

1.1. Social networks

In the construction industry, the materials supply chain is decentralized, and technical knowledge is distributed among independent, competing organizations [10]. At any moment in this complex and unpredictable web of social relations (fig. 1), technical expertise is liable to fragment, forcing the patchwork resolution of technical concerns. Opportunities for integration across functional systems slip by the wayside (fig. 2), increasing the complexity of the materials inventory.

Engineering models must do their work against the background of this shared context. The results of a model can help to establish consensus and steer the activities of other project contributors and stakeholders. For this to happen, the knowledge that the model produces must be compatible with the knowledge and decisions already established or in the processes of being made. Increasing the fidelity of a simulation, for instance, can be a waste of resources if the design parameters suddenly change. In contrast, even a very simplified model can positively shape the early evolution of a project, by helping to characterize desirable traits and configurations. Agreeing how the building ought to perform helps to clarify the basis of technical design and the associated vocabulary, which in turn improves the quality

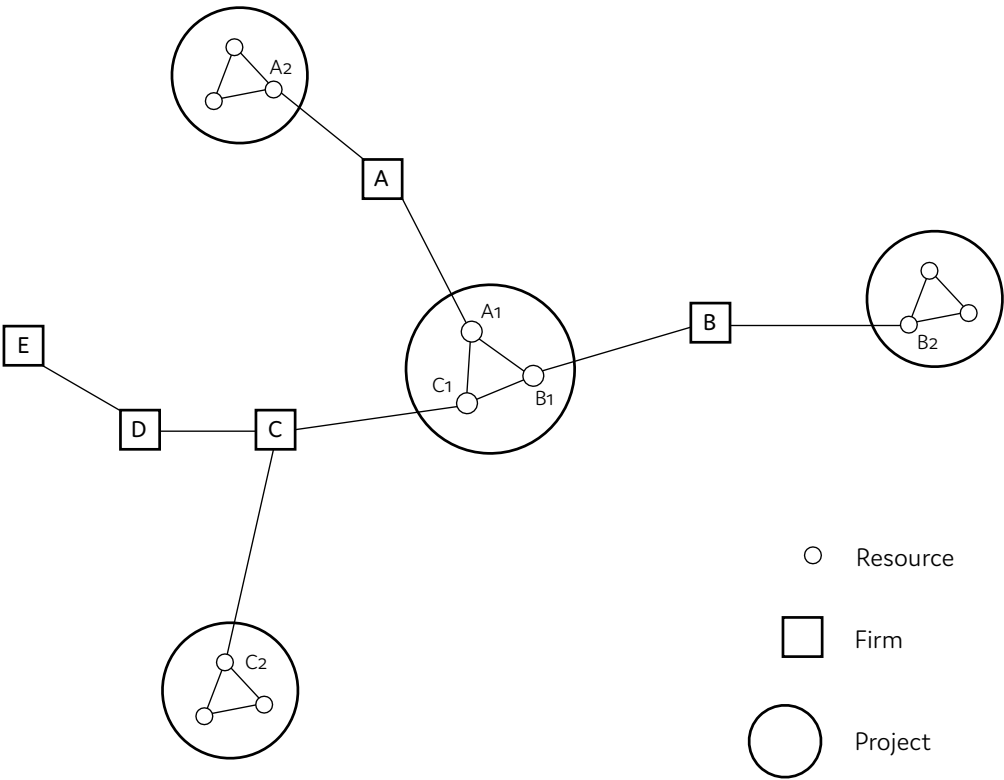


Figure 1: A construction project in its dynamic, social context (adapted from [10]). Firms A, B, and C have different expertise. They must balance their resources competitively and simultaneously across several projects. Technical knowledge is therefore distributed among loosely coupled communities. It can be organized according to any project but is liable to fragment if social relations weaken or breakdown.

of correspondences between more detailed studies, and the people doing them, later on.

In the early stages of design, architects develop a range of volumetric forms to facilitate discussion with project contributors and stakeholders. These so-called "massing studies" do not need to be geometrically detailed; their purpose is to help build consensus on which issues and ideas to prioritize and develop further. Measures for shape compactness [12] and parametric "shoe- box" models [13–17] can help design teams establish the proportions and parameters that govern energy efficiency. These guidelines and studies may be suitable for generic planning, real estate, or renovation projects, but may lose their relevance for cultural landmarks—such as some civic buildings, corporate headquarters, or mixed-use developments—where the team must pay special attention to the form and network of

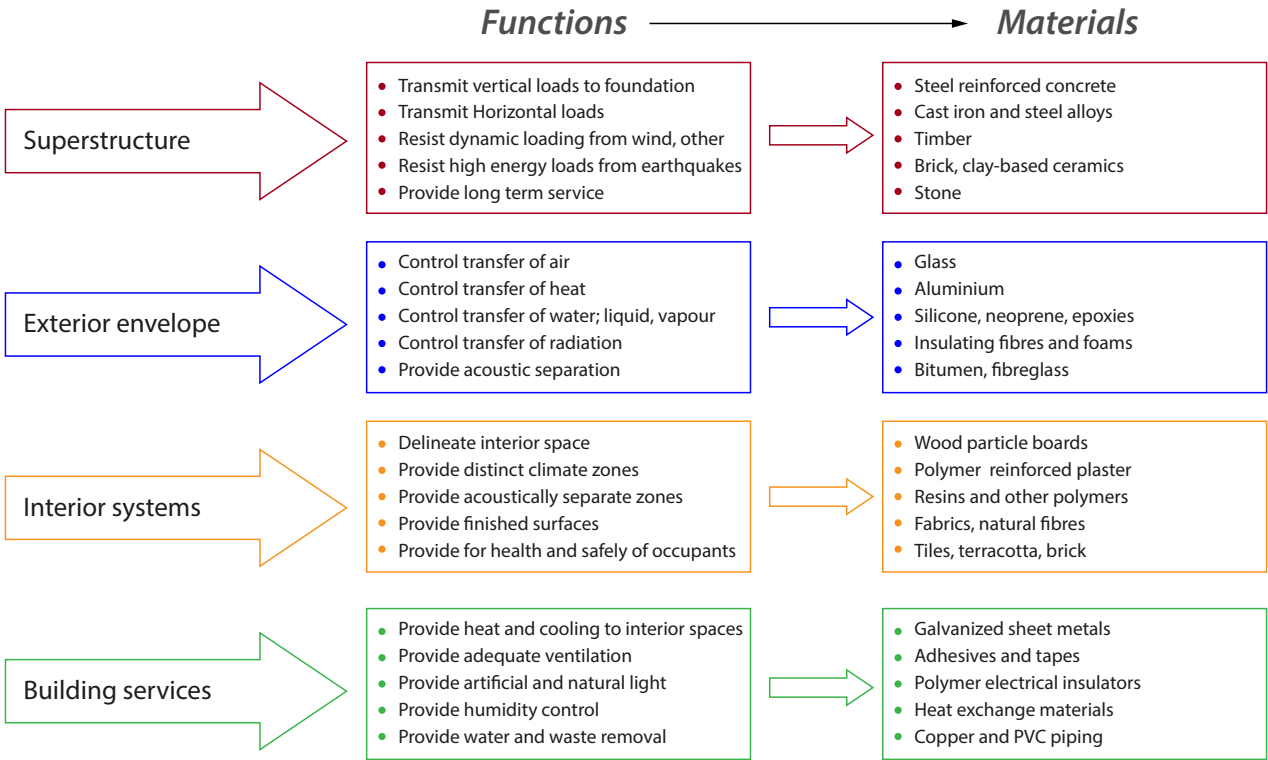


Figure 2: The functional systems of a modern building (adapted from [11]). Dividing up functions in this way helps to organize the expertise and activities of project contributors. But it can also mask opportunities for functional integration, and wastefully increase the size and scope of the materials inventory.

indoor and outdoor spaces to positively shape the inter-subjective experience of people.

As the cut-off point for avoiding runaway climate change draws near, project teams will come under increasing pressure to incorporate hard limits on material quantities and emissions into their initial, malleable designs. In the rush to reconcile these new priorities, some practitioners fear that models of energy efficiency—especially those that cloud their workings from project stakeholders—will come to dominate decision-making to the detriment of design quality. Will these models substitute or serve the imagination [18]? Will models of efficient shoe-boxes become a self-fulfilling prophecy, further compartmentalizing quotidian life and bolstering building practices that are potentially maladaptive [19–21]?

1.2. Strategic models

There are many kinds of thermal models in building design and research, but for this paper, it is possible to distinguish between two kinds, defined by when they happen in the design process. The first kind is a *forecasting* model, built to estimate future patterns of energy use and thermal comfort in absolute terms. Forecasting models require detailed input information: their prediction quality improves as design decisions settle and finalize. The second kind is a *strategic* model, which helps the team to produce and compare design options, and to improve decision-making in the preliminary stages. To be successful, a strategic model must establish what constitutes a well-performing design and show what the requisite balance of technical parameters are—but without predetermining the final design configuration. Strategic models are most effective when they are stripped down to their essential relations so that the causal workings are transparent to all members of the project team and everyone can agree that the model is a suitable proxy for reality.

Experienced analysts may use a strategic model to frame the parameters of debate. For instance, they may treat the model as an opportunity to inform project stakeholders on recent research in adaptive comfort [22–36], advocating for natural ventilation principles to be incorporated into the schematic design. In such a case, the analyst may try to show the cumulative influence of passive design measures on the *floating* or *free-running* temperature; that is, how the interior temperature evolves without active thermostatic control. With the frequency and intensity of heatwaves increasing all over the world [37–39], the free-running temperature provides a basis for sizing cooling plants [40, 41] but also indicates whether interior conditions will stay safely within physiological limits for heat-stress [42, 43], particularly when there is a blackout or when occupants cannot afford to run or install mechanical cooling. Comparing the free-running temperature to thresholds for adaptive comfort and dangerous heat-stress can, therefore, indicate the *thermal resilience* of a proposed design.

1.3. Thermal mass & buoyancy ventilation

When designing buildings for hot climates, *thermal mass* refers to the practice of configuring spaces and materials so that the materials passively store heat during the day then release it at night; as a result, the interior stays naturally cool in the hottest parts of the day [22, 44–48]. Thermal mass is also widely recognized as an opportunity for greater material integration between structural and thermal design [49]. If only the simplicity of some traditional building practices, with mono-material envelopes in stone, brick, wood, or earth, could be reconciled with modern science and expectations. Modern life is increasingly spent indoors with technological accouterments that generate extra heat, while building

envelopes are now composed of several material layers, each with specific functions to accommodate the need for insulation and air-tightness. Where to place thermal mass—The innermost layer? The outermost layer? Both?—is a thoroughly modern question. The most direct way to absorb excess heat generated by interior activities is to expose the mass on the innermost layer (i.e. so it is an "internal mass"). External insulation and shading then protect the mass from the excesses of ambient heat and baking sunshine. However, the absorbed interior heat must somehow be discharged at night for the cooling effect to work the following day. This discharging can be done by ventilation.

Buoyancy ventilation, otherwise known as stack ventilation, refers to the practice of configuring spaces and openings so that the airflow is driven spontaneously by the temperature difference between inside and outside. In updraft mode, warm air rises and escapes out the top while cooler air floods in from below to replace the evacuating air. In downdraft mode, the cycle reverses: cooler air spills out from below and warmer air floods in from above. In recent years, there have been major advances in the engineering theory of buoyancy ventilation, otherwise known as the art of "emptying a filling box" [50–52]. Researchers have solved problems such as how to keep the emptying air from stratifying to save energy on colder days [53, 54], how to differentially size openings in a multistorey building according to the vertical pressure gradient [55, 56], and how to switch to downdraft mode on hotter days with the help of cooling from a concentrated or distributed source [57–60]

Unlike stochastic wind forces, buoyancy forces can be balanced and harnessed in a stable and continuous feedback loop. Sustaining this loop in temperate weather is straightforward. Demand for ventilation exists when people are present: these people and their activities generate heat; this heat can power the ventilation; therefore, balance the temperature and flow rate by sizing the stack and adjusting the openings accordingly. The balancing act is not quite so simple in hot weather. Some cooling is needed to cancel the heat loads and to keep the interior below ambient temperature. Most or all of this cooling can come from thermal mass—so long as the ventilation and heat storage cycles are well synchronized.

1.4. *Thermal massing for the masses*

Built precedents may trick practitioners into believing that thermal massing is a well-understood art [61]. However, a series of recent field studies on termite construction, which revealed that the coupling of mass and buoyancy is solely responsible for the thermal conditioning of some mounds [62–65], serve as a reminder that there is still much to learn.

What proportions should a thermally massive building have? How should the thermal mass be

distributed? Should the "massing" change with the choice of material? The analysis in subsequent sections provides new answers to these questions. The paper outlines a new massing method based on the optimal coupling of thermal mass and buoyancy ventilation. The method allows project teams to compare the functional and environmental credentials of primary construction materials while they evaluate preliminary options for organizing the exterior form and interior spaces of a building. It strategically focuses attention on designing for natural buoyancy ventilation to meet a free-running temperature, and on achieving functional integration with essential materials. Advocates for sustainability may use the method to challenge automatic decisions regarding the use of air-conditioning and the piecemeal design of *ad hoc* material assemblies. The method may also help researchers to identify the proportions and characteristics of thermally resilient buildings in dangerously heating climates.

2. Previous work

This section is written for readers to understand the relevance and limitations of the analysis and method presented in §3 and §4; specialist readers may wish to skip ahead. §2.1 describes the historical and technical context for harmonic lumped parameter models, in relation to other methods used for modelling the effects of thermal mass. §2.2 reviews the literature on the coupling of thermal mass and buoyancy. §2.3 summarizes the harmonic lumped parameter model of Holford and Woods (which serves as the basis of the analysis and method presented in §3 and §4)

2.1. Discretize what?

In 1992, the engineer Philip Niles concluded a review of simulation methods for thermal mass with a prescient observation:

Despite the considerable developments in the harmonic methods, it is doubtful whether the method will compete as a design tool with the finite-difference approach. For most design work, hour-by-hour finite difference simulations appear to be just too fast, flexible, and easy to understand to have any serious competition from the harmonic methods. However, the harmonic method is likely to remain the analytical, as opposed to numerical, approach of choice. Besides its potential accuracy, it produces a rich explanation of why buildings perform the way they do

Philip W. B. Niles, "Simulation Analysis", in [66]

The harmonic method, sometimes called the frequency-response or the admittance method, is based on the Fourier transform equation, which says that any pattern in space and time can be thought of as a superposition of sinusoidal patterns with different frequencies. Joseph Fourier developed this transform technique in the 19th century to solve his famous heat equation [67]. Today, Fourier transforms are used by scientists and engineers across disciplines, who break down component frequencies to analyze data patterns, create them to order, extract essential features, and remove random noise [68].

What distinguishes essential features from noise? Arguably the most direct approach to energy simulation is to work with a literal 3D representation. The digital geometry represents an energy field in Cartesian coordinates, divided into a continuous mesh of smaller volumes. For every solid and fluid element, a set of partial differential equations describing the transport and transformation phenomena associated with that medium are iteratively and simultaneously solved (alongside surface radiation, etc). The smaller the size of each element and the shorter the duration of each time step, the more realistic the physical representation.

Could 'noise' from the smallest vortices, measured in microns and microseconds, nudge the buoyant air circulating an auditorium into a different flow pattern? In the future, will analysts import tomographic scans of actual materials to trace vapour migrating through pores and fibres back to sweat on furrowed foreheads? These questions, while exaggerated, are not entirely fanciful: Chaos theory shows that small perturbations can make a dynamical system evolve entirely differently, while latent heat transfer can dominate the energy balance of a building and produce mould in multi-layer walls. The ultimate expression of the finite-volume approach, which promises a god-like view of every energetic interaction, is not yet feasible in everyday practice. The data-processing demands are still too high. Discretizing these models efficiently is a technical art. Recognized proxies often bridge the gap to small-scale processes, such statistical models for turbulence, or empirical correlations for surface heat transfer.

The question of how to discretize thermal models has occupied building scientists for decades. Most thermal models are not Cartesian representations but topological networks. Many of these thermal networks follow the logic of electrical circuits. The nodes represent the different building components and the various sources and sinks participating in the 'thermodynamic bath'. Questions concerning discretization relate to the number of nodes and connections, and hence the number and kinds of equations to simultaneously solve.

In the second half of the twentieth century, the harmonic analysis of simplified networks promised

180 a shortcut to understand the dynamic response of thermally massive buildings. Harmonic analysis
181 represents heating or cooling at the surface of a mass as one or more sinusoidal 'excitations,' which
182 operate at daily frequencies and resemble real thermal agitations, such as the day-to-night swing in
183 ambient temperature, or the winter sun arcing through a window. With these boundary conditions
184 defined, the heat equation can be broken down analytically into a series of simpler equations containing
185 lumped parameters, which characterize the transient behaviour of the mass. These ratios, known
186 as phase lags and attenuations, have an intuitive physical meaning and neatly summarize how a
187 temperature wave inside the mass will evolve. One insight from applying this method was the discovery
188 of a heat storage limit for internal thermal mass [66, 69] which proved that, contrary to common sense,
189 a thicker mass is not always better. Beyond a certain point, extra thickness compromises the ability of
190 the mass to absorb heat. Today's temperature wave encounters the remnants of yesterday's wave on
191 its journey through the mass. The waves overlap and partially cancel each other out by superposition.
192 This finding was recently revisited and refined by Ma and Wang [70].

193 Building energy simulation programs use statistically averaged climate data and internal load pro-
194 files divided up into hourly (or smaller) time intervals. They therefore need to model the response of
195 thermal mass to staccato heating signals that may bear little resemblance to continuous sine waves.
196 While it is theoretically possible to break down any signal into sine waves using the Fourier transform,
197 programmers of early software found it more efficient to use other transform functions to model tran-
198 sient responses to pulses and steps. For instance, EnergyPlus, one widely used program today, treats
199 transient conduction just as two older programs in its version-history (BLAST and DOE-2) treated
200 it [71]. The default settings employ a transform function known as the Conduction Transform Function
201 to compute a single bulk temperature for multi-layer walls. A CTF operation is similar to a Fourier
202 transform. The heat equation is broken down into a matrix containing time-invariant coefficients (i.e.
203 multiplying factors), which characterize the transient response of the lumped mass. These coefficients
204 are automatically calculated once the physical properties and dimensions of the multi-layer wall as-
205 sembly are defined. The pre-calculated matrix then virtually transforms the lumped temperature at
206 each time-step according to past and present thermal exchanges. This approach means there are fewer
207 computations to do at each time-step once the simulation starts.

208 The main difference between the CTF method and the harmonic method is the abstract 'space'
209 in which the mathematical operations are made. The invariant coefficients in the CTF method are
210 defined in 'state-space', as opposed to phase-lags and attenuations in the 'frequency domain'. Other

traditional state-space methods for transient conduction include the Laplace transform and the z-transform [72–74]. More recently, eigenspace representations, familiar to structural engineers, have also been used [75, 76]. Newer response factor and lumped parameter models use numerical optimization techniques to determine the values of the time-invariant coefficients [76–78].

With computing power readily available, and data-exchange between simulation tools increasingly necessary, response factor methods may eventually become redundant in everyday practice. In many practical cases, a finite-difference (or, equivalently, a finite-volume) model will quickly and accurately iterate for the surface temperature as it co-evolves with radiation, convection, and transient conduction—for every time-step. Knowing the surface temperature is especially important if the aim is to understand the natural conditioning effects of an internal thermal mass. Acknowledging this, EnergyPlus developers have incorporated a finite-difference solver as an optional setting, following the trend set by other simulation tools such as ESP-r [72] or ApacheSim [79] (which forms part of IES).

If Niles was right about the future uptake of numerical methods, what about his predictions regarding harmonic analysis? As highlighted by a recent review on systemic discrepancies between simulations of thermally massive buildings [80], if the team evaluating a simulation does not have the theoretical frame to gauge the quality of results, they may falsely acquire an illusion of certainty, leading them to make poor design decisions. In other words, harmonic analysis may still have an important role to play, helping a new generation to make sense of all the data produced by their detailed numerical models. Moreover, harmonic analysis may continue to provide physical insights—insights that help design teams decide what configurations are worth modelling in the first place.

2.2. Close coupling

In 2003, Yam, Li, and Zheng [81] were the first to examine the non-linear coupling between an internal thermal mass and buoyancy ventilation. Yam *et al.* derived differential equations to describe this non-linear behavior and solved them numerically. The results showed a close-to-periodic variation of the interior temperature. This finding led them to conclude that harmonic analysis could reasonably represent the coupling, assuming an average heat transfer coefficient for the surface.

Inspired by this finding, Holford and Woods [82] undertook a thorough mathematical investigation of the coupling in 2007. They parameterized the relationships between diffusion through an internal mass, convection at its surface, and buoyancy ventilation, and described the relationships in terms of dimensionless ratios (i.e. without units). They then solved the differential equations numerically for a range of scenarios, assuming periodic (i.e. harmonic) variations in the ambient temperature. Using

the same parameters, they then built an approximate lumped model, and systematically compared the results of this approximate model to the more detailed numerical version—and found good agreement. Significantly, their lumped model is discretized into four interacting temperature signals—the exterior temperature, the interior temperature, the surface temperature of the internal mass, and the lumped temperature of the mass. As the review in §2.1 suggests, the ability to accurately estimate the coupled surface and interior temperature—using analytical shortcuts—represents a significant advance in the thermal mass literature.

2

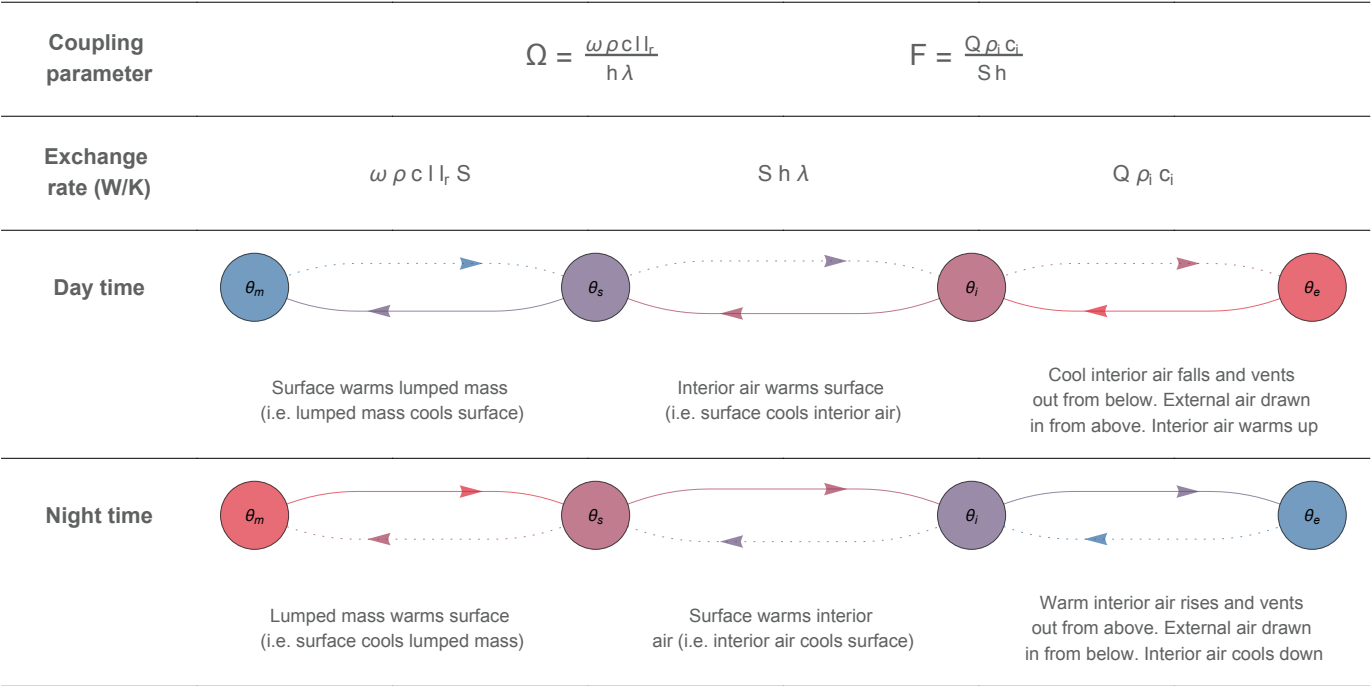


Figure 3: The natural feedback loop between internal thermal mass and buoyancy ventilation, as parameterized by Holford & Woods [82]

In 2008, unaware of the work of Holford and Woods, Zhou *et al.* [83] added to the work of Yam *et al.* (Li was a common co-author) by outlining a method to solve for the interior surface temperature, based on harmonic analysis. Their approach also considered periodic losses and gains from exterior insulation (both Yam *et al.* and Holford and Woods had assumed adiabatic boundary conditions, i.e. perfect insulation). In 2011, interested in the effects of massive floors, ceilings, and furniture, Zhou *et al.* [84] showed how to bundle the buffering effects of different pieces of thermal mass into a 'virtual sphere'. This approach posed the question: why relegate thermal mass to the envelope at all?

In 2009, Lishman and Woods [85] characterized thresholds for how natural ventilation behaves in

thermally massive buildings. These thresholds depend on the unsteady balance between buoyancy forces, wind forces, interior heating, and heat storage. They found that the balance of these forces plays out on short and long time-scales, making for a surprising range of possible evolutionary paths and final flow regimes. For instance, if the interior heat load suddenly changes, the regime may rapidly switch from wind-driven to buoyancy-driven flow, only to switch back hours later once the thermal mass adjusts to the changes. Understanding these path-dependencies is important, so that they can be strategically avoided or harnessed by design. In 2012, unaware of this work (but citing other important works, e.g. [86–88]), Faure and Roux [89] analyzed the short and long term effects that thermal mass has on natural displacement ventilation, focusing on features such as the stratification height and how this interface buoys or "overshoots" before settling to steady-state.

In chapter 4 of his textbook on buoyancy ventilation published in 2013 [90], Chenvidyakarn took the findings of [58, 60] and neatly summarized how the strength of buoyancy ventilation in downdraft mode depends on the ratio of cooling from a thermal mass compared to competing heat loads. In 2016, Yang and Guo [91] analyzed the coupling between internal mass and buoyancy ventilation using Fourier components at multiple frequencies, to understand the temperature evolution of the system when driven by more realistic ambient conditions—that is, an exterior temperature signal which is not quite sinusoidal. Comparing their predictions to data from a small physical experiment, they confirmed that these more realistic excitations produced ventilation flow rates that are *anharmonic* (but which are nevertheless predictable with Fourier analysis).

In 2018, Bastien and Athienitis [92, 93] gave a skilled demonstration of how to design thermal mass inside greenhouses and solaria. They did some parametric design studies using the frequency response method (combining Laplace transforms and Fourier analysis), then followed this up with detailed annual simulations using the finite-difference method. The parametric studies allowed them to compare different approaches to optimizing the thermal mass thickness, arguing that the best approach for solaria was to control the delay between when the mass absorbs most sunshine and when it releases this heat. If Bastien and Athienitis had come across the work of Holford and Woods, might they have also been tempted to see what thermal mass looks like when optimized for buoyancy ventilation?

As §2.1 and §2.2 show, plenty of new knowledge has been published in the thermal mass literature since the turn of the century, especially for efficient methods to simulate thermal mass in arbitrary configurations. However, it seems that none of this new knowledge has been integrated and distilled into a workable set of parameters, to help architects and planners proportion thermal mass buildings

properly in light of the challenges posed by climate change. Of all the studies on thermal mass, the work by Holford and Woods seems to be the most promising as a basis for the necessary design guidance.

2.3. The Holford and Woods model

Figure 3 describes the feedback loop between thermal mass and buoyancy ventilation, as modelled and parameterized by Holford and Woods [82]. The parameters F and Ω are dimensionless numbers (i.e. they are ratios without units). They control the relative heat exchange between ventilation and thermal mass, respectively. When $F \sim \Omega \sim 1$, the heat exchange between the ventilation and the thermal mass is balanced. When $\Omega \gg F$, the thermal mass dominates—the interior temperature is highly damped, and the air changes are relatively low. When $F \gg \Omega$, the ventilation dominates—the air changes are relatively high, and the thermal mass hardly affects the interior temperature.

The two ends of the casual chain in figure 3 are unconnected, and this highlights one of the most significant simplifications in the Holford and Woods model. The model assumes an internal mass, meaning there is no heat transfer at the outer face. There is no direct thermal contact between the mass and the external environment; there is only an indirect connection via the interior air. These adiabatic boundary conditions are equivalent to perfect exterior insulation, or adjacent spaces with perfectly replicated thermal conditions.

Figure 4 shows the influence of F and Ω on the interior, surface, and mass temperatures during a 24-hour cycle. The temperature signals are normalized, so they are relative to maximum 1 and minimum -1 while the time is expressed in radians. The outside temperature varies periodically:

$$T_e(t) = T_0 + \Delta T \cos(\omega t) \quad (2.1)$$

Where T_0 is the mean daily temperature, $T_0 = (T_{min} - T_{max})/2$, ΔT is the temperature increment above the mean, $\Delta T = |T_{max} - T_0|$, and ω is the angular frequency, $\omega = 2\pi/86400$. The dimensionless time is:

$$\tau = \omega t \quad (2.2)$$

The dimensionless temperature is:

$$\theta = \frac{(T - T_0)}{\Delta T} \quad (2.3)$$

The four temperatures in the system are defined as follows. The exterior temperature:

$$\theta_e = \cos(\tau) \quad (2.4)$$

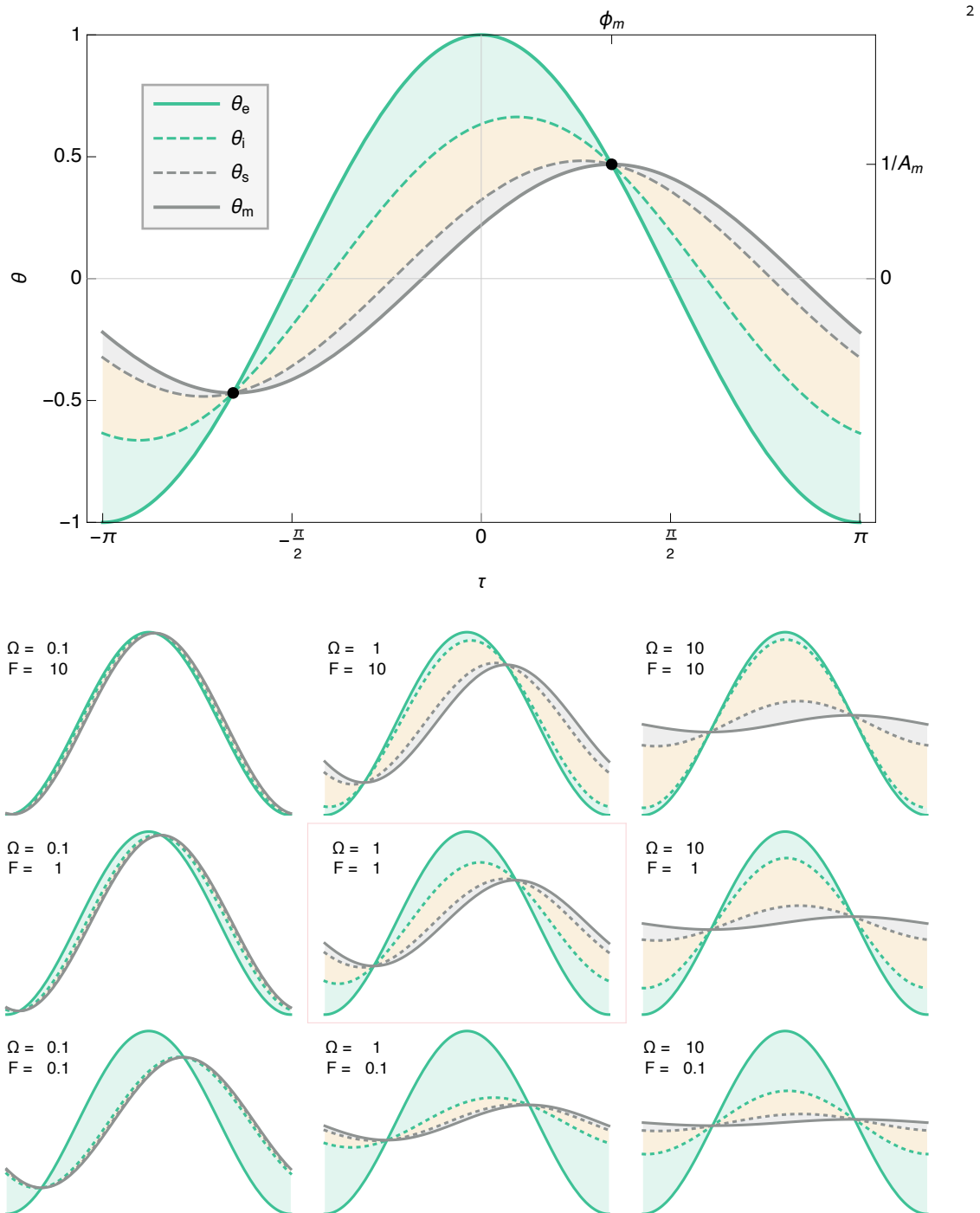


Figure 4: The influence of the ventilation parameter F and the massing parameter Ω on the relative floating temperatures, θ_i , θ_s , θ_m (i.e. interior, surface, mass), driven by cyclic changes in the external temperature θ_e over a period of $2\pi = 24$ hours, after Holford & Woods [82]. The surface temperature delay of the thermal mass is arbitrarily fixed at $\lambda = 0.75$ in all graphs.

312 The interior temperature (assuming perfectly mixed air):

$$\theta_i = \frac{\cos(\tau - \Phi_i)}{A_i} \quad (2.5)$$

313 The surface of the thermal mass facing the interior:

$$\theta_s = \frac{\cos(\tau - \Phi_s)}{A_s} \quad (2.6)$$

314 And the temperature of the thermal mass:

$$\theta_m = \frac{\cos(\tau - \Phi_m)}{A_m} \quad (2.7)$$

315 The thermal mass is modelled as a lumped mass, meaning that, unlike a real mass, there are no
 316 temperature gradients inside it. A lumped mass has a single evolving temperature that represents the
 317 equivalent work of a real mass. The lumped mass temperature signal is close to, but not the same
 318 as, the average temperature of a real mass. Significantly (as discussed in §2.2 and contextualized in
 319 §2.1), Holford and Woods were also able to find a shortcut to defining the surface temperature. (They
 320 did this by formulating the parameter λ , see Equation (2.24).) In this way, it was possible to get an
 321 accurate representation of the coupling between the mass-surface-interior without having to solve for
 322 the temperature gradients inside the mass at different time intervals.

323 To plot the temperature signals, one needs to know the attenuation (A) and the phase lag (Φ). The
 324 reciprocal of the attenuation ($1/A$) is the peak temperature, relative to $\theta_e = 1$. The phase lag is the
 325 time delay of the peak temperature, relative to $\tau = 0$. The attenuation for the interior temperature
 326 is:

$$A_i = \frac{A_m}{\sqrt{1 + \Omega^2}} \quad (2.8)$$

327 The attenuation for the surface temperature is:

$$A_s = \frac{A_m}{\sqrt{1 + \Omega^2(1 - \lambda)^2}} \quad (2.9)$$

328 And the attenuation for the mass temperature is:

$$A_m = \frac{1}{\cos(\Phi_m)} \quad (2.10)$$

329 The parameters λ and Ω will be defined shortly. The phase lag of the interior temperature is:

$$\Phi_i = \Phi_m - \tan^{-1}(\Omega) \quad (2.11)$$

330 The phase lag of the surface temperature is:

$$\Phi_s = \Phi_m - \tan^{-1}((1 - \lambda)\Omega) \quad (2.12)$$

331 Algebraic substitution reveals that the temperature definitions all include Φ_m :

$$\theta_i = \sqrt{1 + \Omega^2} \cos(\Phi_m) \cos(\tau - \Phi_m + \tan^{-1}(\Omega)) \quad (2.13)$$

$$\theta_s = \sqrt{1 + (1 - \lambda)^2 \Omega^2} \cos(\Phi_m) \cos(\tau - \Phi_m + \tan^{-1}((1 - \lambda)\Omega)) \quad (2.14)$$

$$\theta_m = \cos(\Phi_m) \cos(\tau - \Phi_m) \quad (2.15)$$

332 How to solve for the mass phase lag, Φ_m ? The first option is to numerically solve the differential
333 equations that define their lumped parameter model:

$$\begin{aligned} \Omega \frac{d\theta}{d\tau} &= \theta_i - \theta_m \\ 0 &= \lambda(\theta_m - \theta_i) + F(\theta_e - \theta_i) |\theta_e - \theta_i|^{1/2} \end{aligned} \quad (2.16)$$

334 Alternatively, Holford and Woods found two shortcuts for estimating Φ_m :

$$\left(\frac{\tan(\Phi_m)}{\Omega} - 1 \right)^6 = \left(\frac{\lambda^2}{\Omega F^2} \right)^2 \left(1 + \frac{1}{\Omega^2} \right) (1 + \tan^2(\Phi_m)) \quad (2.17)$$

$$\frac{\tan(\Phi_m)}{\Omega} = 1 + 1.07 \left(\frac{\lambda^2}{\Omega F^2} \right)^{1/3} \quad (2.18)$$

335 They compared the accuracy of Equation (2.16), Equation (2.17), and Equation (2.18) against a full
336 numerical model (which represented diffusion through the mass with finite-differences and which al-
337 lowed the ventilation to vary non-linearly). They found that Equation (2.16) and Equation (2.17) stay
338 accurate to within 0.1% and 1%, respectively, across parameter space—even for very extreme scenarios
339 (e.g. when a very thick mass combines with a very high rate of ventilation, leading the surface temper-
340 ature to stray far from the mass temperature). Equation (2.18) is less consistent; it is only reasonably
341 accurate for balanced scenarios.

342 Since Φ_m is determined by parameters Ω , λ , and F , these three parameters alone control the entire
343 system. The massing parameter Ω is defined as:

$$\Omega = \frac{\xi(\cosh(2\eta) - \cos(2\eta)) + \eta(\sinh(\eta) - \sin(2\eta))}{\eta(\sinh(2\eta) + \sin(2\eta))} \quad (2.19)$$

Where ξ is the potential rate of heat storage compared to the rate of surface heat transfer:

$$\xi = \frac{\omega \rho c l}{h} \quad (2.20)$$

And l is the thickness of the mass, ρc is the volumetric heat capacity of the mass material, and h is the surface heat transfer coefficient. The parameter η is the ratio of the layer thickness to the depth of thermal penetration :

$$\eta = l \sqrt{\frac{\omega}{2\alpha}} \quad (2.21)$$

Where α is the thermal diffusivity of the mass material. Note that the Biot number, traditionally used to assess whether a lumped mass model is appropriate, is $Bi = 2\eta^2/\xi$. However, as discussed previously, by solving the surface temperature, Holford and Woods found a way of accounting for temperature gradients inside the mass without having to further discretize the model; hence checking the Biot number is unnecessary. The massing parameter can also be written as:

$$\Omega = \frac{\xi l_r}{\lambda} = \frac{\omega \rho c l l_r}{h \lambda} \quad (2.22)$$

Where l_r is the fraction of material thickness needed for the lumped mass to do the equivalent work of the real mass:

$$l_r = \frac{(\cosh(2\eta) - \cos(2\eta))}{\eta (\sinh(2\eta) + \sin(2\eta))} \quad (2.23)$$

And λ is a factor which, by approximating the temperature gradients inside the mass, determines the surface temperature:

$$\lambda = \frac{1}{1 + \frac{\eta (\sinh(2\eta) - \sin(2\eta))}{\xi (\cosh(2\eta) - \cos(2\eta))}} \quad (2.24)$$

This surface temperature factor ranges between $0 < \lambda < 1$. When $\lambda = 1$, there are no temperature gradients inside the mass, so $\theta_s = \theta_m$. When $\lambda \rightarrow 0$, the surface temperature strays further and further away from the mass temperature; as a result, the mass stores heat less and less efficiently.

Finally, we can define the ventilation heat exchange parameter, which compares the ventilation heat exchange to the surface heat exchange at the surface:

$$F = \frac{Q \rho_i c_i}{S h} \quad (2.25)$$

Where $\rho_i c_i$ is the volumetric heat capacity of air, S is the surface area of mass exposed to the interior air, and the rate of ventilation, Q , is:

$$Q = A^* \sqrt{\beta g H |T_e - T_i|} \quad (2.26)$$

Where A^* is the effective area of ventilation openings (see [94]), β is the thermal expansion coefficient of air, and H is the stack height. The rate of ventilation, powered by buoyancy, depends on the interior temperature—which in turn depends on the rate of ventilation. This feedback mechanism is described in figure 3. Holford and Woods suggest setting $|T_e - T_i| = \Delta T$ in Equation (2.26) to obtain a reference ventilation rate. Alternatively, we define an average ventilation rate, based on the normalized mean temperature difference:

$$Q = A^* \sqrt{\beta g H \Delta T |\theta_e - \theta_i|_{mean}} \quad (2.27)$$

According to the integral mean value theorem, the mean temperature difference is:

$$|\theta_e - \theta_i|_{mean} = \frac{1}{b-a} \int_a^b |\theta_e - \theta_i| d\tau \quad (2.28)$$

Where $b = \Phi_m - \pi$ and $a = \Phi_m$ mark the beginning and end of half a cycle. Substituting equations Equation (2.4) and Equation (2.13) and completing the integration gives:

$$|\theta_e - \theta_i|_{mean} = \frac{-2\Omega \cos(\Phi_m) + 2\sin(\Phi_m)}{\pi} \quad (2.29)$$

3. Analysis

§2 showed that, while there has been lots of progress on efficient methods for simulating the effects of thermal mass in arbitrary configurations, none of this knowledge has been integrated and distilled into a workable set of parameters, to help architects and planners proportion thermal mass buildings properly. The work by Holford and Woods [82] provides a basis for the much-needed design guidance. Using their parametric definitions, this section finds a new way to optimally synchronize the coupling of internal thermal mass and buoyancy ventilation.

3.1. The optimal tuning

The lumped parameter model of Holford and Woods [82], summarized in §2.3, describes the coupling between internal thermal mass and buoyancy ventilation. This coupling is controlled by two non-dimensional parameters: F/λ (the ratio of ventilation heat transfer to surface heat transfer) and Ω (the ratio of thermal storage to surface heat transfer). This section defines two optimal tunings for F/λ and Ω . The two optimal tunings are associated with different damping coefficients, defined graphically in Figure 5.

The first damping coefficient is the maximum difference between the interior and exterior temperature in a given cycle, $|\theta_e - \theta_i|_{peak}$. Let us call it the *peak venting temperature difference*, since it is

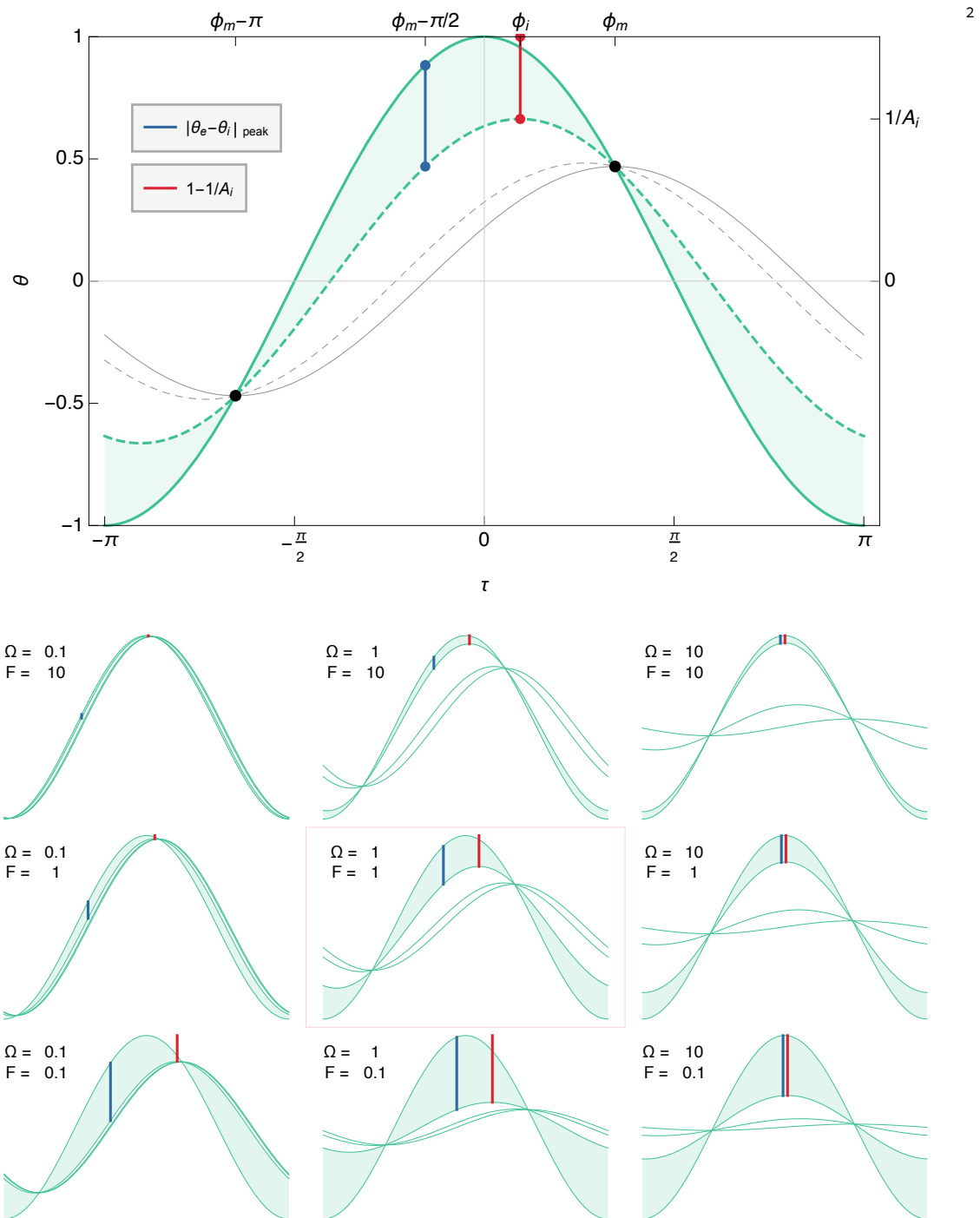


Figure 5: The definition of two damping coefficients: the peak venting temperature difference, which is shown in blue and occurs at time $\tau = \Phi_m - \pi/2$, and the attenuating temperature difference, $1 - 1/A_i$, which is shown in red and occurs at time $\tau = \Phi_i$. The graphs show the influence of F and Ω on both kinds of damping coefficient. The surface temperature delay of the thermal mass is arbitrarily fixed at $\lambda = 0.75$ in all graphs.

the moment of maximum buoyancy ventilation. It occurs twice in a 24-hour cycle, but when exactly? As indicated in figures 4 and 5, all temperatures in the system converge at time $\tau = \Phi_m$. When this happens, the buoyancy ventilation momentarily ceases before switching direction from a daytime downdraft to a nocturnal updraft. If the minimum venting temperature difference occurs at time $\tau = \Phi_m$, it follows that the peak venting temperature difference occurs midway through a half-cycle at time $\tau = \Phi_m - \pi/2$. Subtracting equation 2.12 from 2.4 and substituting the definition for τ gives:

$$|\theta_e - \theta_i|_{peak} = -\Omega \cos(\Phi_m) + \sin(\Phi_m) \quad (3.1)$$

Now is necessary to substitute a definition for Φ_m . As discussed in §2.3, Equation (2.18) is less accurate than Equation (2.17), but it does have the advantage of not needing to be solved iteratively. Moreover, recall from §1.3 that strategic comparisons, not absolute forecasts, are the focus of this paper. Substituting Equation (2.18) gives:

$$|\theta_e - \theta_i|_{peak} = \frac{1.07 \left(\frac{\lambda^2}{F^2 \Omega} \right)^{1/3} \Omega}{\sqrt{1 + \left(\Omega + 1.07 \left(\frac{\lambda^2}{F^2 \Omega} \right)^{1/3} \Omega \right)^2}} \quad (3.2)$$

Figure 6 shows a contour plot of the peak venting temperature difference as a function of F/λ and Ω . Notice how, for every increment of $|\theta_e - \theta_i|_{peak}$, there is an optimal pairing of Ω and F/λ . This ideal tuning is defined by the curve:

$$(F/\lambda)_{max} = \sec(1.07\Omega^{4/3}) - 1 \quad (3.3)$$

Optimal design values can be found by solving Equation (3.2) and Equation (3.3) simultaneously. To do this, one needs to consider F/λ as a single variable in Equation (3.2) (i.e. so that $\left(\frac{\lambda^2}{F^2 \Omega} \right) = \left(\frac{1}{a^2 \Omega} \right)$, where $a = F/\lambda$). The independent values for F and λ can be found later. For instance, solving Equation (3.2) and Equation (3.3) tells us that to optimize for $|\theta_e - \theta_i|_{peak} = 0.5$, one should design the thermal mass such that $\Omega = 0.94$; this will maximize the F/λ parameter such that $F/\lambda = 0.83$. Now recall that λ predicts the surface temperature delay due to temperature gradients inside the mass, and depends on the choice of the material. If calculations for one material show that $\lambda = 0.9$, then $F = 0.83 * 0.9 = 0.747$ (see §4.1 for a more detailed example).

In this way, one can evaluate the effect of the thermal properties of materials fairly. All material masses can be sized to achieve the same optimal value for the massing parameter Ω —it is just a matter of finding the correct thickness. However, because of differences in thermal properties, different material

masses can't have the same values for both Ω and λ . The differences in λ manifest as differences in surface temperature, and the surface temperature regulates the power of buoyancy ventilation. Therefore, everything else being equal, materials with a lower λ are less efficient as thermal mass because they produce less ventilation.

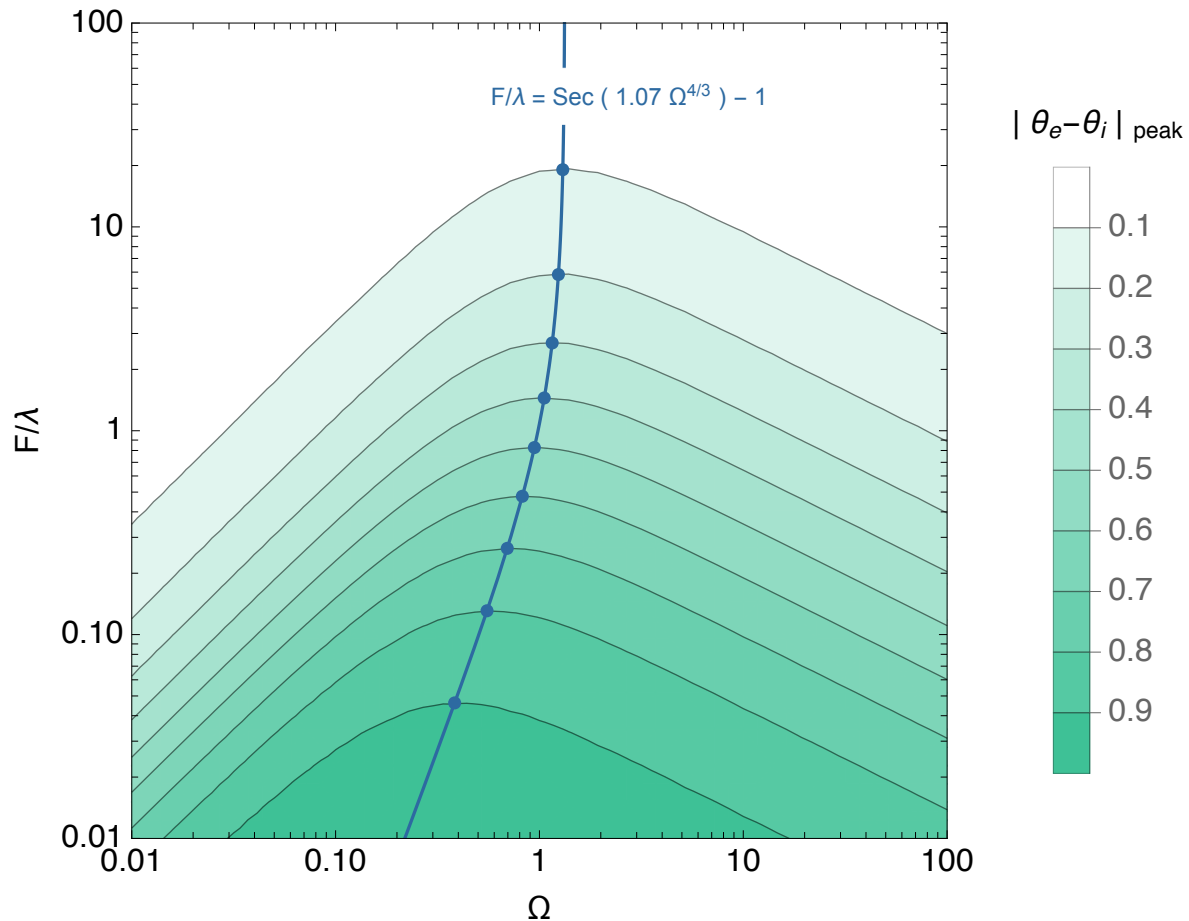


Figure 6: Contour plots of the peak venting temperature difference $|\theta_e - \theta_i|_{peak}$. The blue curve locates the optimal pairings of Ω and F/λ

Figure 5 defines a second damping coefficient, which occurs at time $\tau = \Phi_i$. Let us call it the attenuating temperature difference:

$$1 - \frac{1}{A_i} = 1 - \sqrt{1 + \Omega^2} \cos(\Phi_m) \quad (3.4)$$

Substituting equation 2.11 gives:

$$1 - \frac{1}{A_i} = 1 - \frac{\sqrt{1 + \Omega^2}}{\sqrt{1 + \left(\Omega + 1.07 \left(\frac{\lambda^2}{F^2 \Omega} \right)^{1/3} \Omega \right)^2}} \quad (3.5)$$

Figure 7 shows a contour plot of the attenuating temperature difference as a function of F/λ and Ω . Once more, notice how, for every temperature increment, there is an optimal value of Ω for which F/λ is maximized. This ideal tuning is defined by the curve:

$$(F/\lambda)_{max} = \tan\left(\frac{1.07}{2}\Omega^{4/3}\right) - 1 \quad (3.6)$$

Like before, optimal design values can be found by solving Equation (3.5) and Equation (3.6) simultaneously. For instance, to achieve $1 - 1/A_i = 0.5$, one should design the thermal mass such that $\Omega = 1.62$; this will maximize the ventilation parameter such that $F/\lambda = 0.61$.

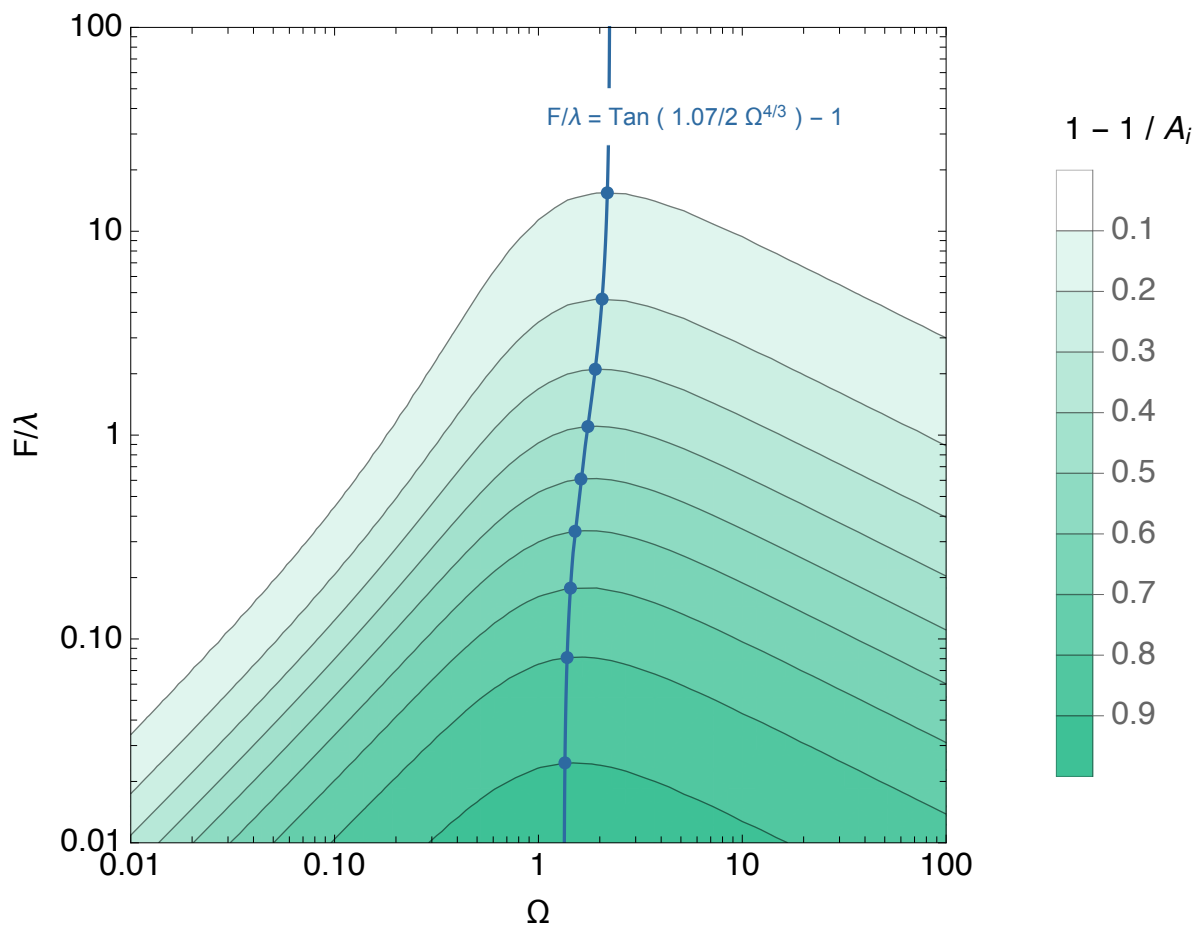


Figure 7: Contour plots of the attenuating temperature difference $1 - 1/A_i$. The blue curve locates the optimal pairings of Ω and F/λ

Notice that the optimal values for both damping coefficients are quite similar. The attenuating temperature difference is associated with slightly larger values for optimal Ω and slightly smaller values for maximum F/λ . These small differences in the ideal tuning can have a large impact on the physical dimensions of the architecture, as the massing studies of §4 will show.

3.2. Surface heat transfer

The previous subsection described how to optimize thermal mass and natural ventilation in a feedback cycle, by finding ideal pairs F/λ and Ω to synchronize the coupled heat exchanges. Section 3 explores the implications of these ideal proportions for sizing buildings and choosing materials. However, before doing this, a fair estimate of the surface heat transfer coefficient, h , is essential, as both F/λ and Ω depend on it. This subsection also shows how to adjust h to approximately account for internal loads.

At the surface of an internal mass, sensible heat exchange occurs by convection and radiation. The rate of convection determines the strength of coupling between the thermal mass and buoyancy ventilation. Any radiation heat transfer has an indirect, but consequential, influence on this coupling.

Surface convection inside rooms can be driven naturally by surface temperatures, forcibly by nearby air flows, or by a mixture of natural and forced convection. Forced convection on an interior surface may be a consequence of breeze from fans, vents, and open windows, plumes from warm people and equipment, or a larger circulation pattern powered by buoyancy inside the space. In this paper, natural convection is the focus. Unlike forced convection, natural convection is guaranteed to happen in the thermal feedback cycle described in this paper, and will do so in synchronization with the temperature evolution of the system. If there is a particular scenario in which forced convection may be significant, its influence on the baseline natural convection can be estimated by consulting the correlations in the literature [95–97], or by running high-resolution transient simulations with computational fluid dynamics incorporating the thermal energy equation [98].

As the contour plot in figure 8 shows, the heat transfer coefficient for natural convection varies according to the interaction between thermal and gravitational forces. The heat transfer coefficient is smallest when the orientation of the surface ($\gamma \rightarrow 180^\circ$) impedes warm air from rising or cool air from falling. In other orientations, the heat transfer coefficient is larger. Turbulence ensues when viscous forces no longer dominate, and the boundary layer de-laminates from the surface.

Figure 8 was computed using an algorithm recommended by Raithby and Hollands (see [99, 100]). The algorithm evaluates five empirical correlations for the heat transfer coefficient: a pair of correlations for surfaces at inclination $\gamma = 0^\circ$ (one for laminar flow, one for turbulent flow); a pair for surfaces at inclination $\gamma = 90^\circ$ (laminar and turbulent); and one for surfaces at inclination $\gamma = 180^\circ$ (gravity keeps the flow practically quiescent in this case). For intermediate angles (e.g. $\gamma = 77^\circ$), some other equations combine results from two reference angles (e.g. $\gamma = 0^\circ$ and $\gamma = 90^\circ$) after balancing their

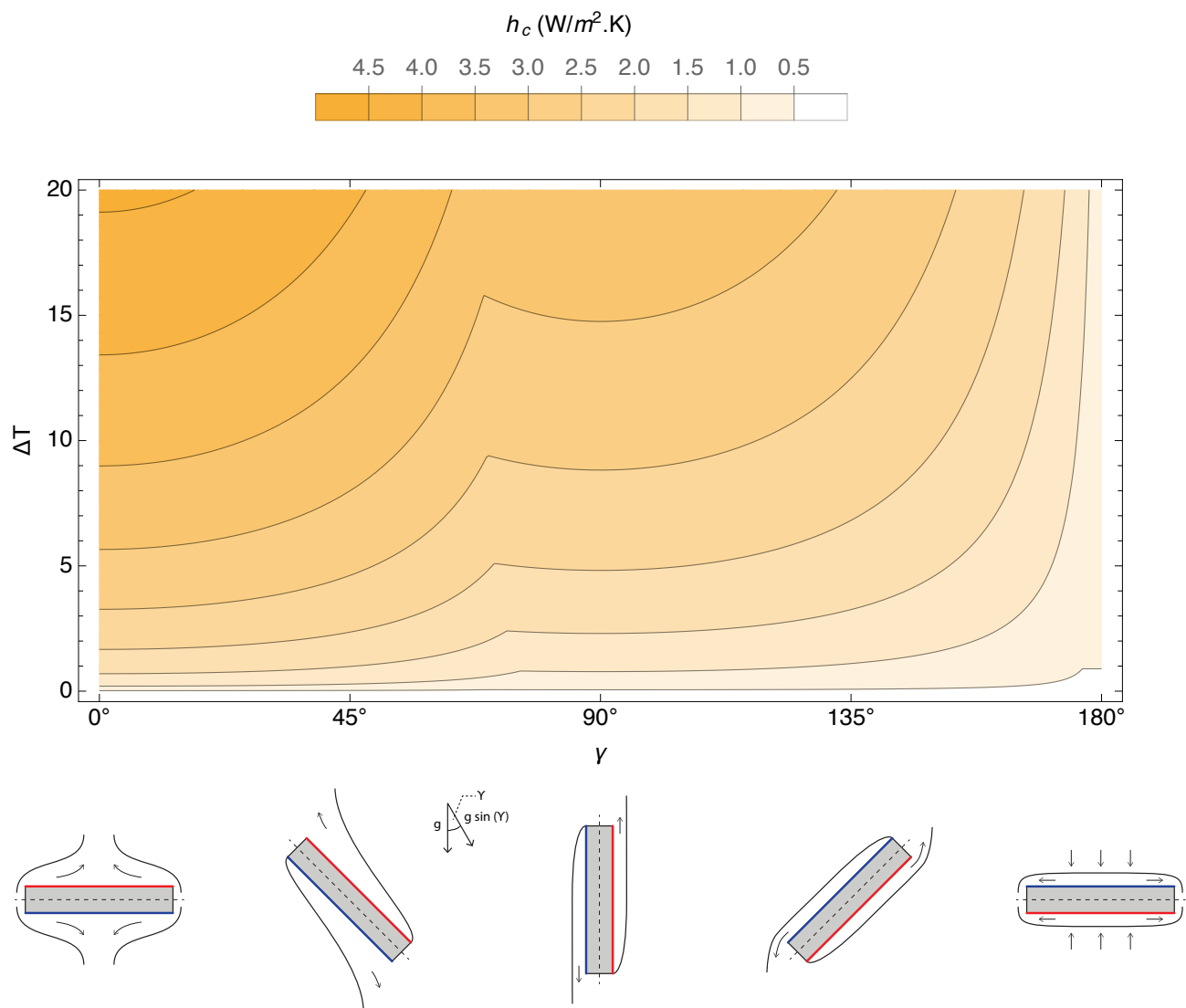


Figure 8: Contours of the average heat transfer coefficient, h , due to natural convection from a hot or cold surface. It varies according to the temperature difference, the rotation angle, and the size of the surface (here 3 x 3 m).

weights asymptotically. The five empirical correlations are not shown here. However, with some minor exceptions, they all take the general form:

$$Nu = \frac{h_c k}{L} = m Ra^n \quad (3.7)$$

Where Nu is the Nusselt number, h_c is the average heat transfer coefficient for natural convection, k is the thermal conductivity of the fluid (in this case, air), L is the characteristic length of the surface (e.g. the ratio of the area to the perimeter), n is a fraction less than 1 (usually 1/4 or 1/3), m is an

empirically derived constant, and Ra is the Rayleigh number:

$$Ra = \frac{g \beta L^3 (T_s - T_i)}{\nu \alpha} \quad (3.8)$$

Where ν and α are the viscosity and the thermal diffusivity of the air, respectively. While conducting the calculations, the influence of the characteristic length (L) was evidently weak for panel sizes bigger than approximately 1 by 1 meter. Mathematically speaking, the weakening influence of L is because the exponent n in Equation (3.7) asymptotically levels out the influence of the Rayleigh number (even though $Ra \propto L^3$). Physically speaking, air is not very viscous: on a large surface, the natural convection boundary layer soon reaches full turbulence, even if powered by a small temperature difference. Therefore, figure 8 (which assumes a surface of 3 by 3 meters) can be used to approximate the natural heat transfer coefficient for many surface sizes inside rooms, at any inclination, from concrete table tops to triple-height walls.

For a more complete estimate of the average convection heat transfer coefficient, it is necessary to know the mean temperature difference between the surface and the interior. According to the integral mean value theorem:

$$|\theta_i - \theta_s|_{mean} = \frac{1}{b-a} \int_a^b |\theta_i - \theta_s| d\tau \quad (3.9)$$

Where $b = \Phi_m - \pi$ and $a = \Phi_m$ mark the beginning and end of half a cycle. Substituting equations 2.14 and 2.15 and completing the integration gives:

$$|\theta_i - \theta_s|_{mean} = \frac{2 \lambda \Omega \cos(\Phi_m)}{\pi} \quad (3.10)$$

The average surface heat flux can now be defined as:

$$q_{mean} = h \Delta T |\theta_s - \theta_i|_{mean} \quad (3.11)$$

Where h is the total heat transfer coefficient:

$$h = h_c + h_r \quad (3.12)$$

And h_r is the radiation heat transfer coefficient:

$$h_r \simeq \sigma \varepsilon 4 T_0^3 \quad (3.13)$$

Where σ is the Stefan-Boltzmann constant and ε is the average emissivity of the surfaces. Equations (3.11) and (3.12) assume that surface radiation, like surface convection, is governed by the

temperature difference between the surface and the interior. Let us interrogate the validity of this assumption by imagining an idealized scenario. Consider a fictional body inside the space that follows the interior temperature and exchanges radiant energy uniformly with all surrounding surfaces. This fictional radiator does not heat the air directly, but it does heat the air indirectly at a later time (because it heats or cools the mass, and later the mass heats or cools the air). Consider also that when there is no radiator present, and the idealized space is empty, there is no net radiation exchange between the enclosing surfaces since they are all the same temperature.

3.3. Interior heat loads

Can this fictional radiator be used as a proxy for internal heat loads? In a real room, there are many kinds of heat sources and sinks, of different sizes, locations, and time signatures. Locally, they heat or cool the interior air by convection. Remotely, they heat or cool other surfaces by radiation. Real interior heat loads are not evenly distributed in space, nor are they harmoniously synchronized in time. Moreover, recall that the direction of heating for the fictional radiator is $\theta_i > \theta_s$ during the day, switching to $\theta_i < \theta_s$ during the night. Real interior heat loads may diminish or disappear at night, but they do not spontaneously turn into sources of cooling.

Despite these inconsistencies and contradictions, a fictional radiator (which follows the interior temperature) is still a relevant proxy for average heat loads. This radiator cannot represent realistic heating distributions in time or space, because a harmonic model cannot account for the possible knock-on effects of asymmetrical or asynchronous loads on the temperature evolution of the system. Nevertheless, evaluating the effects of an average heat load is a useful starting point. Once the team have settled on the schematic design, the engineer can interrogate this assumption with a more detailed model incorporating more realistic load profiles.

To apply this proxy for internal heat loads, the analyst must first evaluate the heat flux from the fictional radiator and decide if it needs increasing to meet any deficit in the expected average heat load. Meeting the deficit can be done by multiplying h_r by some factor. Then the analyst must imagine a plausible scenario for the charging and discharging cycles to remain balanced over the day. For instance, by assuming that the ventilation openings (A^*) are automatically increased at night, so the extra buoyancy ventilation matches the night cooling by the fictional radiant body.

Figure 9 compares the cumulative surface heat transfer due to natural convection and radiation. The yellow portions of the graph show natural convection, which is present even when the interior space is empty. The red parts show emissions from a fictional radiator as a proxy for internal loads.

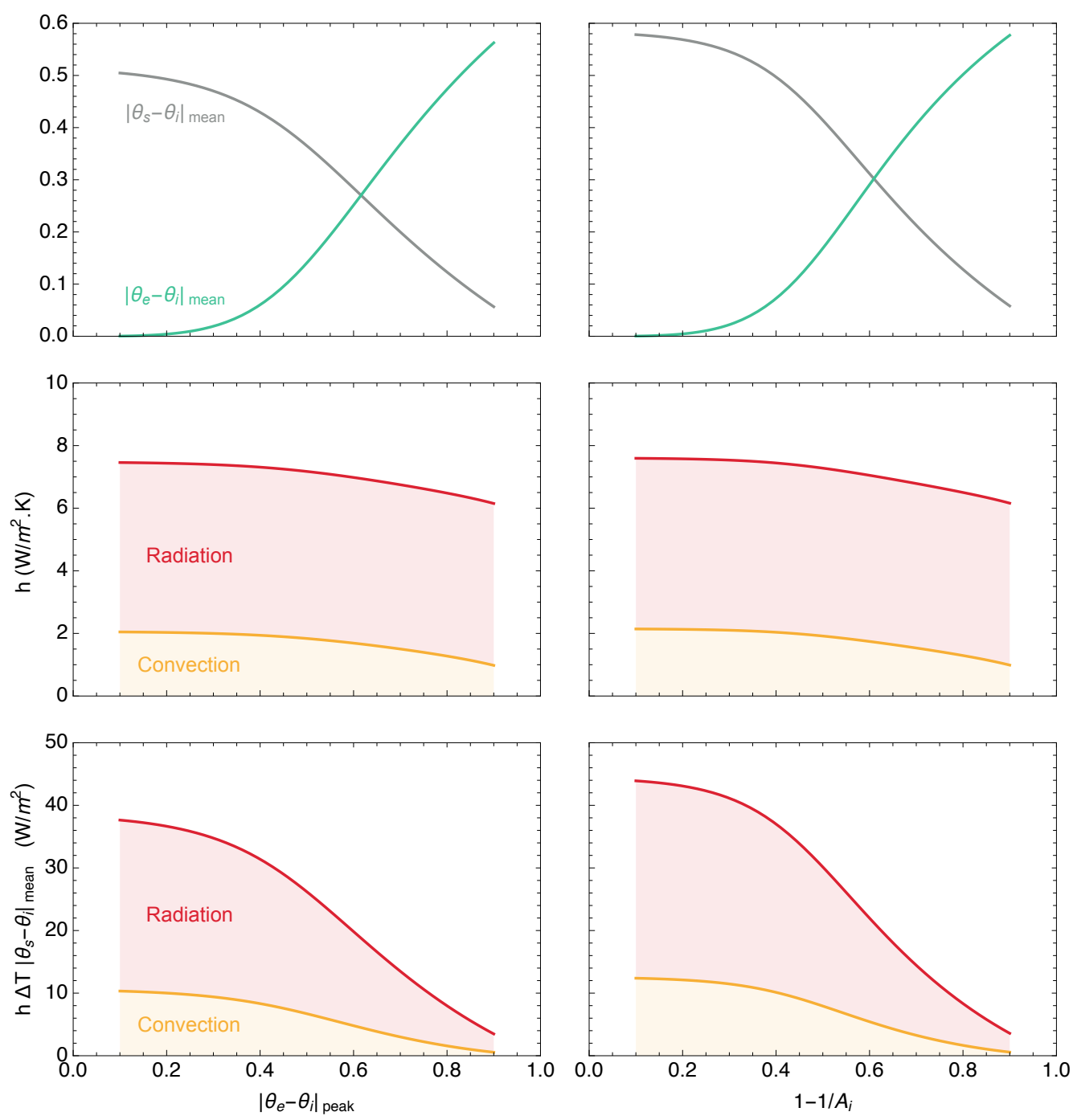


Figure 9: Variation of surface heat transfer with $|\theta_e - \theta_i|_{peak}$ and $1 - 1/A_i$

The graphs are arranged in a grid with two columns, one for each damping coefficient: the left-hand column aligns with the peak venting temperature difference $|\theta_e - \theta_i|_{peak}$; the right-hand column aligns with attenuating temperature difference $1 - 1/A_i$. The top row of graphs shows a governing trend: the larger the damping coefficient, the smaller the temperature difference between the surface and the interior air. This downturn leads to slight reductions in the heat transfer coefficient ($\text{W}/\text{m}^2\text{-K}$, see middle row), but considerable reductions in the surface heat flux (W/m^2 , see bottom row).

Note that, in figure 9, the radiant heat transfer coefficient is defined by equation Equation (3.13), and the radiant heat flux is controlled by $|\theta_s - \theta_i|_{mean}$ in Equation (3.11). In other words, the radiant heat flux has *not* been adjusted to equally represent internal loads for all values of either damping coefficient. In this way, the relative changes and possible deficits are clear to see. Furthermore, note that the heat flux is reported in terms of the unit surface area of the mass, not in terms of the unit floor area (which is how internal loads are typically presented).

To compute the results shown in figure 9, the environmental temperature was fixed at $\Delta T = 10$ and $T_0 = 20^\circ\text{C}$ (293.15 K). Optimal pairs of F/λ and Ω are needed to calculate $|\theta_s - \theta_i|_{mean}$ for increments of $|\theta_e - \theta_i|_{peak}$ and $1 - 1/A_i$. This was done by simultaneously solving Equations (3.2) and (3.3) or Equations (3.5) and (3.6), assuming no surface temperature delay (i.e. $\lambda = 1$). The surface heat transfer was then computed following the procedure described in §3.2, assuming a large, 10 by 10 meter vertical surface for the convection calculations. The same assumptions and procedures for calculating surface heat transfer and proxy loads are used in the massing studies in the next section (§4).

Table 1: Candidates for thermal mass: representative ranges for thermal properties and CO₂ footprints [101]

	k ($\text{W}/\text{m-K}$)	ρc ($\text{J}/\text{m}^3\text{-K}$)	CO ₂ footprint (kg/m^3)
Steel	51.5 ± 2.5	$(3.79 \pm 0.20) \times 10^6$	$14135. \pm 875.$
Sandstone	5.70 ± 0.30	$(2.16 \pm 0.28) \times 10^6$	$87. \pm 19.$
Concrete	1.6 ± 0.8	$(2.3 \pm 0.4) \times 10^6$	$260. \pm 53.$
Glass	1.00 ± 0.30	$(2.22 \pm 0.15) \times 10^6$	$1850. \pm 142.$
Brick	0.59 ± 0.14	$(1.49 \pm 0.29) \times 10^6$	$402. \pm 82.$
Hardwood*	0.46 ± 0.05	$(1.59 \pm 0.18) \times 10^6$	-400 ± 1300

*Values for k assume conduction is parallel to the grain. Values for CO₂ footprint range from net storage to net release. Notice how, per unit volume, timber can sequester carbon or be worse than concrete, depending on how the forest is managed.

4. Results and discussion

The previous section described the Holford and Woods model, used it to find optimal pairings for F/λ and Ω , and explained how to approximately account for internal loads by adjusting the heat transfer coefficient. This theory is now applied in some massing studies, which show the effect that optimal designs have on material quantities and physical proportions.

4.1. Materials comparison

Among practitioners, it is common knowledge that some materials are more effective as thermal mass because of their thermal properties. (Namely: the thermal conductivity, k (W/m-K); the volumetric heat capacity, ρc (J/m³-K); and the combination of these in a ratio called the thermal diffusivity, $\alpha = k/\rho c$ (m²/s), which compares the internal rate of heat transfer to heat storage, indicating how quickly heat spreads through a material.) However, when it comes to examining thermal mass materials in action, it is difficult to draw conclusions that meaningfully influence design—particularly in the critical early stages—since it is hard to isolate the role that architectural properties play in the co-evolution of system temperatures. What proportions should a thermally massive building have? How should the thermal mass be distributed? Should the massing change with the choice of material? Without comprehensive answers to these questions, analysts, when studying the effects of thermal mass with dynamic models, have had little choice but to fix the dimensions of their control buildings arbitrarily [14, 102, 103]—until now.

Table 1 gives ranges of thermal properties for some standard construction materials [101]. Figure 10 compares the efficiency of these materials as thermal mass when they are optimally tuned as part of a thermal feedback cycle (c.f. fig. 1)—that is, a building with internal mass that maximizes buoyancy ventilation for a given damping coefficient ($|\theta_e - \theta_i|_{peak}$, light shading; $1 - 1/A_i$, dark shading). Figure 10 shows the layer thicknesses (l , bottom row) and the divergence in surface temperatures (λ , top row) for different materials. The width of the coloured bands reflects the uncertainty associated with the thermal properties (c.f. Table 1); the dotted lines assume average values for these properties.

Figure 10 is based on the same set of assumptions as figure 9, which are described in the last paragraph of §3.3. That is, figure 9 shows the heat transfer coefficients and heat fluxes involved in the computations for figure 10. Recall that the radiant heat flux varies with $|\theta_s - \theta_i|_{mean}$; it was *not*

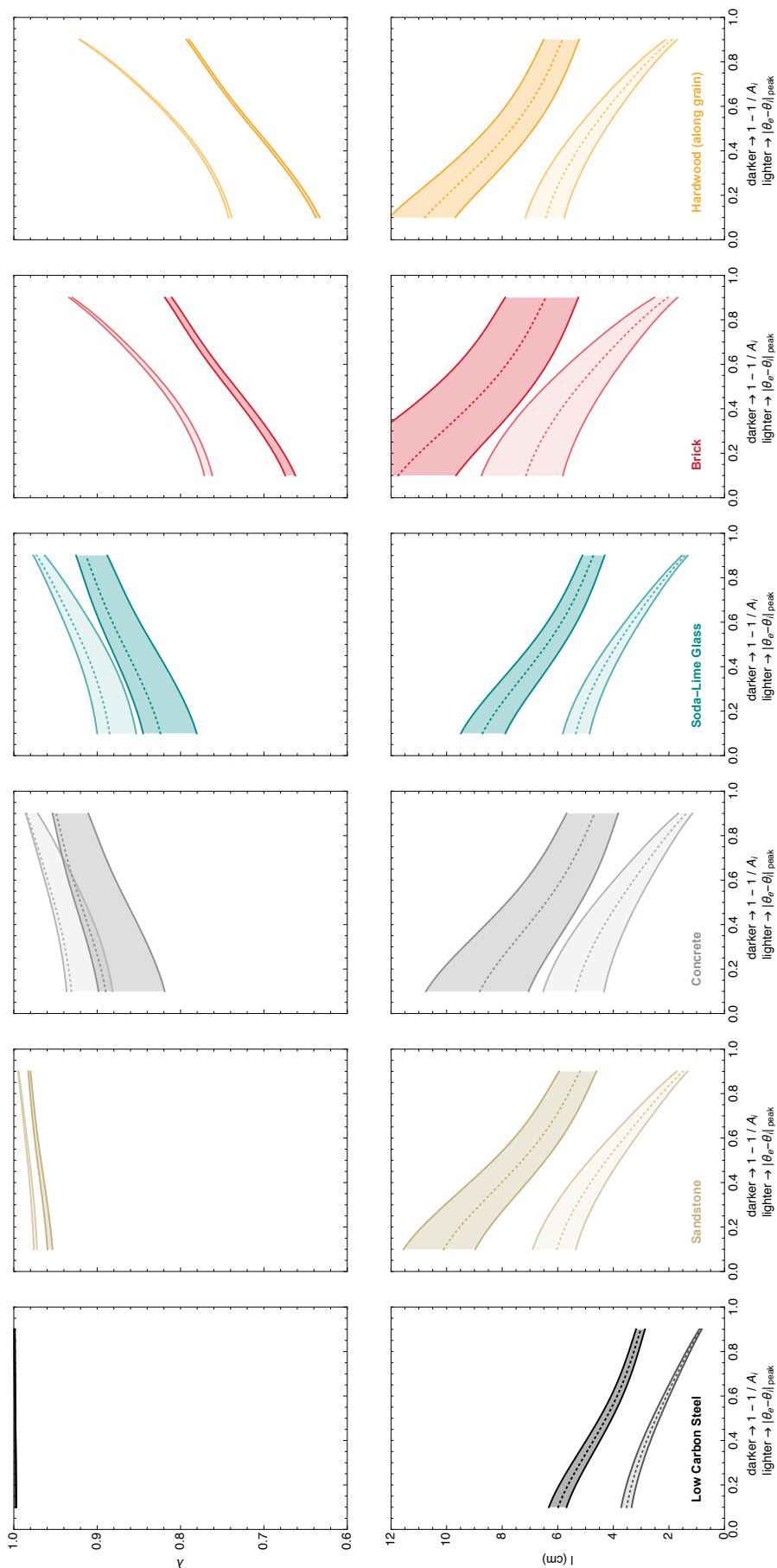


Figure 10: Optimal thicknesses (l) and resulting surface temperature lags (λ) for various construction materials as a function of the damping coefficient, $|\theta_e - \theta_i|_{peak}$ (light shading), or $1 - 1/A_i$ (dark shading). The coloured bands depict the variation in thermal properties reported in Table 1.

adjusted to model internal loads equally across all values of the damping coefficient. Figure 10 can be reproduced with different inputs by following these three steps:

- Choose a damping coefficient to optimize for ($|\theta_e - \theta_i|_{peak}$ or $1 - 1/A_i$) and find the associated optimal values for Ω (c.f. §3.1)
- Estimate h by: (a) Consulting figure 8 and figure 9. Or (b) estimate $|\theta_s - \theta_i|_{mean}$ by setting $\lambda = 1$. Use this result to estimate h (c.f. §3.2), incorporating an estimate for internal heat loads as necessary (c.f. §3.3).
- Find the optimal thicknesses (l) and resulting surface temperature delays (λ) by simultaneously solving Equations (2.22), (2.23) and (2.24). (A first approximation can be made by assuming $\lambda = 1$, so that $l_r = 1$ and Equation (2.22) reduces to $\Omega = \xi$)

Figure 10 reveals some general trends, which reflect the balance of thermal relationships

- As either damping coefficient ($|\theta_e - \theta_i|_{peak}$ or $1 - 1/A_i$) increases, the optimal thickness reduces. This is because the massing parameter, Ω , and the surface heat flux, $h \Delta T |\theta_s - \theta_i|_{mean}$, reduce, too.
- Optimizing for the damping coefficient $|\theta_e - \theta_i|_{peak}$ results in relatively thinner masses, because this damping coefficient is associated with smaller values of Ω , and so requires less thermal capacity.
- The uncertainty associated with thermal properties can lead to significant discrepancies in optimal thickness—in the order of centimeters. In later stages of design, it is therefore important to obtain more accurate values for thermal properties, ideally with direct measurements of actual samples.

Moreover, figure 10 suggests several new findings regarding the efficiency of different construction materials as thermal mass:

- Some natural stones and concretes are particularly efficient as an internal thermal mass when optimally-tuned, which should come as no surprise since these materials have relatively high k and high ρc . However, the ideal tuning adds new meaning to what constitutes an efficient thermal mass. The plots show that, when optimized, sandstone and concrete have non-divergent surface temperatures ($\lambda \rightarrow 1$). Recall that $F = (F/\lambda) * \lambda$. Therefore, compared to other optimized

masses, these masses are able to produce more ventilation for a given damping coefficient (c.f. §3.1)

- However, some concretes (those with lower k and ρc) do not perform as well. The function for λ (Equation (2.24)) is particularly sensitive in the range $1 \lesssim \eta \lesssim 2$ (c.f. fig 8.b. in Holford and Woods [82]). Optimally-tuned concrete is uniquely situated in this range, making it susceptible to sudden (and unexpected) drops in efficiency. Consider that the thermal properties of concrete (or any structural material for that matter) are rarely specified or measured in real projects.
- The graphs reveal many situations in which $l \lesssim 5$ cm, suggesting that thin-shell structures of minimum weight [104–110] may also be optimized for thermal mass and natural ventilation.
- Assuming the heat-flux is oriented parallel to the grain, optimally-tuned hardwood compares well against brick and not too poorly against concrete. (The thermal conductivity of hardwood perpendicular to the grain, and for softwoods in either grain orientation, are lower.) This suggests it is possible to use some timbers as internal thermal mass—with reasonable effect. These thermally resilient timber buildings could legitimately sequester carbon dioxide, so long as the timbers are sourced from sustainable, managed forests, and the buildings last longer than the growing cycles of these forests [101, 111–114].
- While not analyzed here, the thermal properties of earthen materials [115] and high-density bamboo composites [116] suggest that these materials are promising candidates, too.

4.2. Fixed volume of material

The previous subsection compared the efficiency of thermal mass materials when they are optimized in a thermal venting feedback cycle. The remainder of this section examines the consequences of this ideal tuning in terms of building dimensions, material quantities, and ventilation rates.

Figure 11 shows how to distribute *a fixed amount* of concrete thermal mass inside an insulated cuboid of height $H = 10\text{m}$. The floor area is variable, but constrained to the shape of a square (W^2), thereby defining the geometry of the ceiling and four walls where the mass is distributed. Since $V = S l$, optimally distributing a fixed volume of material (V) means finding the balance of surface area (S) and thickness (l) that:

- Meets a given damping coefficient (i.e. a design value for $|\theta_e - \theta_i|_{peak}$ or $1 - 1/A_i$), while;

- Maximizing the rate of buoyancy ventilation (Q).

The calculation flow for producing figure 11 follows these steps:

- Find the ideal tuning for Ω and F/λ (c.f. §3.1)
- Estimate h and find l and λ (c.f. §4.1)
- Now $S = V/l$
- And $Q = \frac{F S h}{\rho_i c_i}$ (c.f.)
- Furthermore, though not shown in figure 11, $A* = \frac{Q}{\sqrt{\beta g H \Delta T |\theta_e - \theta_i|_{mean}}}$ (c.f. eqn. 2.25)

Here are some things to bear in mind when reading figure 11:

- The concrete mix assumes mean values for thermal properties shown in table 1. The environmental temperature and the rates of surface heat transfer are the same as those described in §2.4 and shown in figure 9.
- For the purposes of demonstration, the volume of concrete is arbitrarily fixed at $V = \{8, 27, 64\} \text{ m}^3$.
- For reference, when the ratio of width to height is $W/H = \{1, 2, 3, 4\}$, the surface area of the thermal mass is $S = \{500, 1200, 2100, 3200\} \text{ m}^2$
- For reference, a sufficient amount of ventilation for one person is typically 10 liters per second. That is, $Q = 0.01 \text{ m}^3/\text{s}$. Therefore, when the ventilation rate is $Q = \{0.1, 1, 10\} \text{ m}^3/\text{s}$, there is enough fresh air for approximately $\{10, 100, 1000\}$ people.

Some general observations can be made:

- Optimizing for the attenuating temperature difference requires thicker masses, resulting in smaller buildings (than the peak venting temperature difference if the material volume is fixed).
- The relative power distribution, shown in the bottom row of graphs, does not change with the volume constraint (since the balance of thermal exchanges is the same for each optimal case).

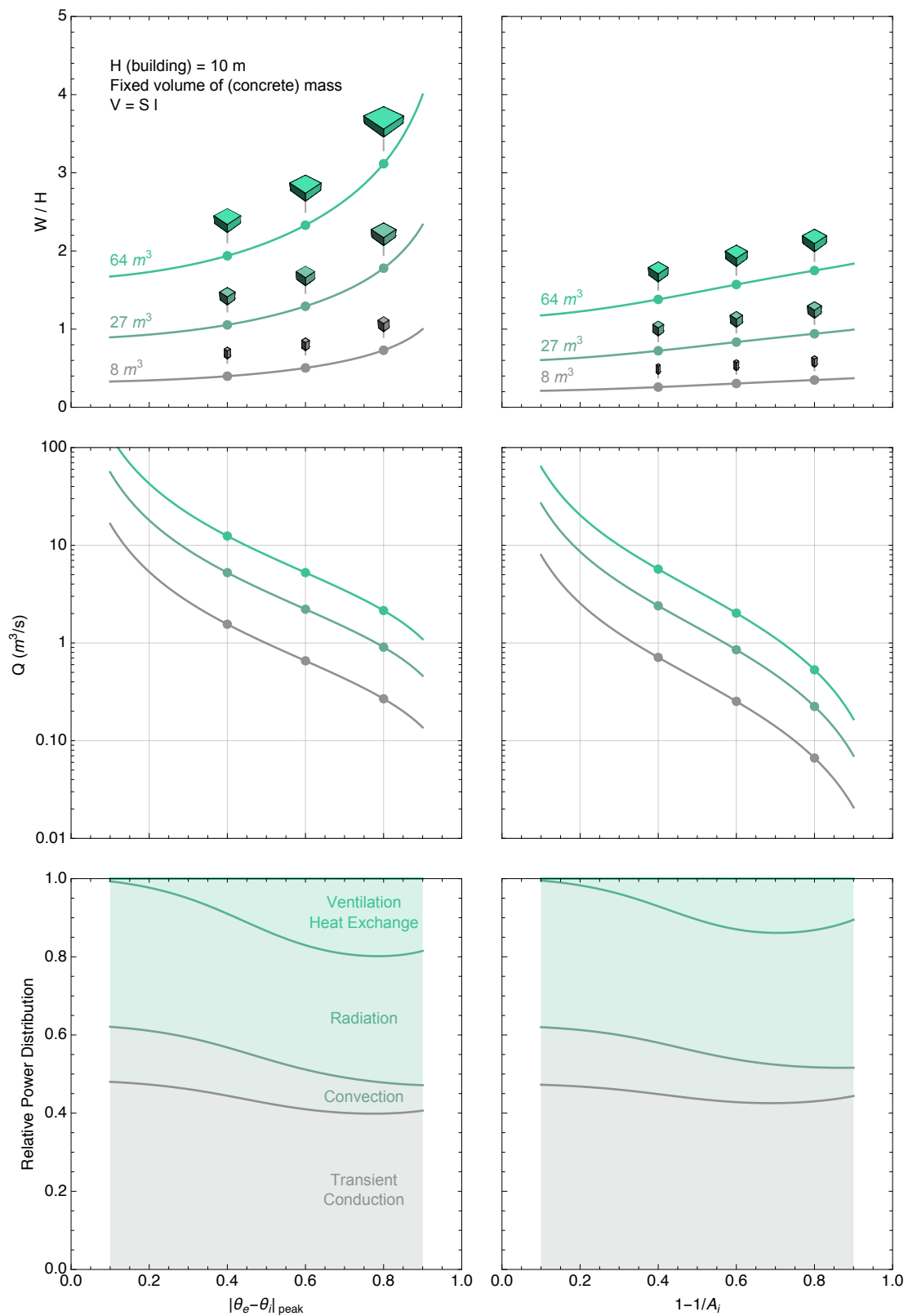


Figure 11: The optimal distribution of a fixed amount of concrete thermal mass ($V = S \text{ l}$) that maximizes buoyancy ventilation (Q) for a given damping coefficient ($|\theta_e - \theta_i|_{\text{peak}}$ or $1 - 1/A_i$)

Figure 11 is a simple demonstration, showing one way of applying the ideal mass tuning in a parametric study. A thermal massing study like this may inform conversations early on in the design process, helping the team to simultaneously establish criteria for architectural proportions, space allocation, temperature damping, natural ventilation, materials selection, material quantities, and carbon emissions. While it is unconventional to fix the amount of material *a priori* design, this strategy may be useful in the coming decade as carbon caps become better defined and more stringent.

4.3. Fixed rate of ventilation

Having shown how to use the ideal tuning to compare massings made from the same volume of material, this subsection compares ideally-tuned massings that produce the same ventilation.

Figure 12 shows how to distribute *the ideal amount* of concrete thermal mass inside an insulated cuboid of height $H = 10\text{m}$. The floor area is variable, but constrained to the shape of a square (W^2), thereby defining the geometry of the ceiling and four walls where the mass is distributed. The rate of buoyancy ventilation is fixed at $Q = \{1, 10\} \text{ m}^3/\text{s}$ to provide enough fresh air for approximately $\{10, 100\}$ people. Since $V = S l$, finding the ideal volume of concrete (V) means finding the combination of surface area (S) and thickness (l) that:

- Meets a given damping coefficient (i.e. a design value for $|\theta_e - \theta_i|_{peak}$ or $1 - 1/A_i$), while;
- Meeting the target rate of buoyancy ventilation (Q).

The calculation flow for producing figure 12 follows these steps:

- Find the ideal tuning for Ω and F/λ (c.f. §2.2)
- Find l and λ (c.f. §3.1)
- Now $S = \frac{Q \rho_i c_i}{F h}$ (c.f. Equation (2.25)) and $V = S l$
- Furthermore, though not shown in figure 11, $A^* = \frac{Q}{\sqrt{\beta g H \Delta T |\theta_e - \theta_i|_{mean}}}$ (c.f. Equation (2.27))

Here are some things to bear in mind when reading figure 12:

- The assumptions (thermal properties, environmental temperature, surface heat transfer) are the same as in figure 11.

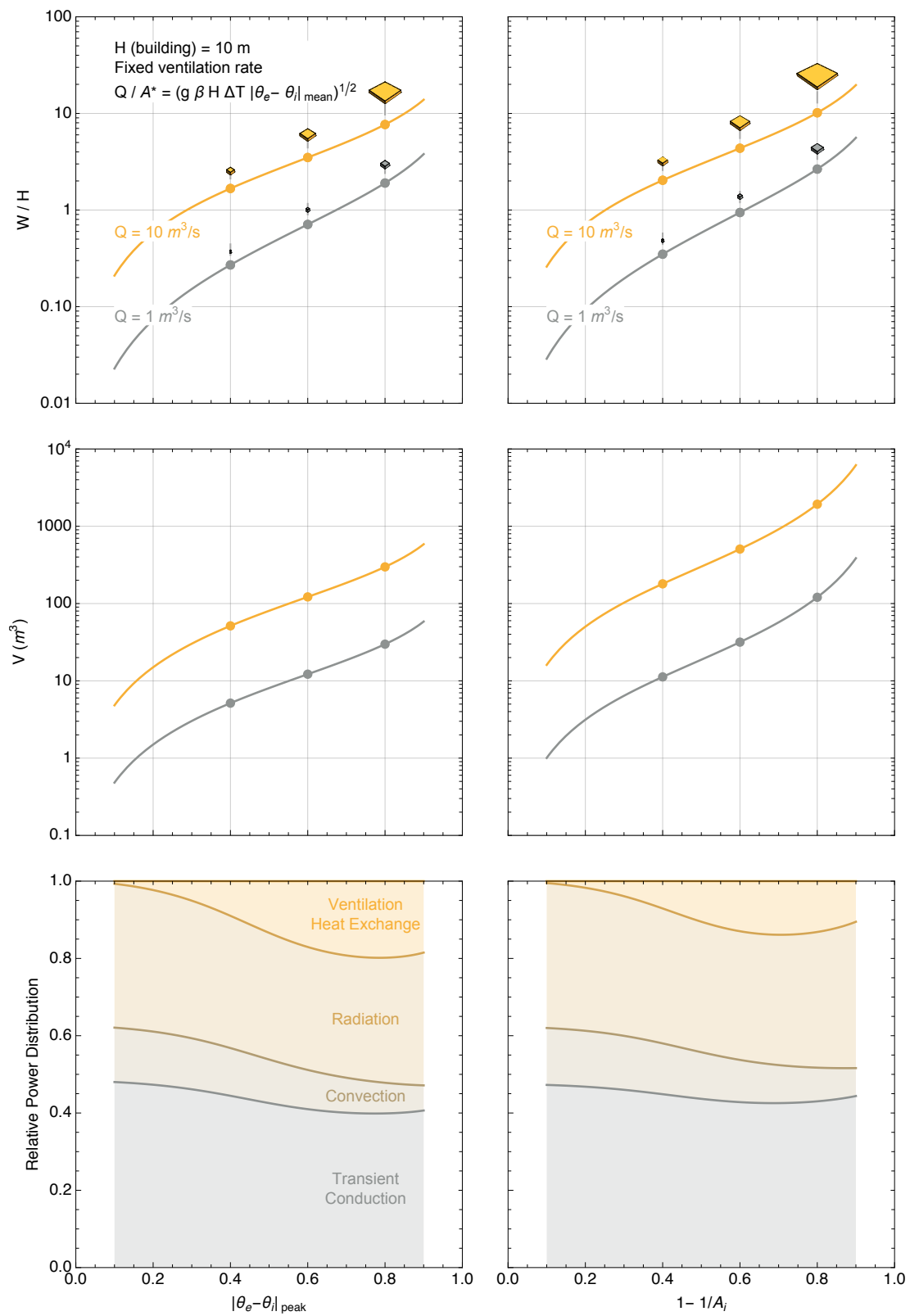


Figure 12: Optimal quantities ($V = \text{Sl}$) and distributions (W/H) of thermal mass for a fixed ventilation rate (Q) to meet a target interior floating temperature ($e-i$ peak or $1-1/A_i$).

- Unlike figure 11, the vertical axis for W/H is logarithmic, as the aspect ratios vary considerably more
- The images of the cuboids are scaled to the largest cuboid in the graph (hence they appear smaller than the cuboids in figure 11).

Compared to figure 11, the ideal proportions (W/H) in figure 12 vary considerably, since there is no constraint on the material volume. One range worth taking a closer look at is the range of damping coefficient $0.6 \lesssim 1 - 1/A_i \lesssim 0.8$ when $Q = 1 \text{ m}^3/\text{s}$. These massings perform well without needing a very large surface ($W/H < 10$) or a very large amount of concrete ($V < 100\text{m}^3$)

Figure 13 interrogates this range in more detail, using different geometries and comparing the efficacy of concrete to timber (hardwood, parallel to the grain, c.f. Table 1) as internal thermal mass. The buildings start as a hemisphere or a cube ($H = 10 \text{ m}$). Their shapes then 'morph' according to mathematically defined rules, which allow the surface area of the building to increase without annexing much extra land. As the surface area increases, so does the damping coefficient—though the ventilation is always the same. Bluer colours, therefore, indicate cooler buildings.

Figure 13 shows three columns of "morph sequences". These morphologies are defined as follows:

- **Blobs.** These surfaces are defined by the Legendre polynomial $P_n(x)$ [117], plotted in spherical coordinates, such that: the radius is $r = 1 + c P_n(\cos(\phi)) \cos(\vartheta)$; the zenith (latitude) angles are $0 \leq \phi \leq \pi$; and the azimuth (longitude) angles are $0 \leq \vartheta \leq \pi$. The coefficient c (here set to $c = 1/4$) determines the "smoothness" of the polynomial and hence the smoothness of the blob. The integer n increases the number of operations in the polynomial and hence the number of "wings" the blob has.
- **Castles.** The remaining two columns are populated by surfaces defined by fractals: a Sierpiński space-filling curve [118], and a Cesàro fractal [119]—which in this case is made by drawing a Koch curve [120] with angles of 85° .

These morphologies are stylistically distinct, which serves to show that, while the ideal tuning for thermal mass governs bulk dimensions, material quantities, temperature attenuation, and buoyancy ventilation, it does not overly determine the choice of form or the spatial layout. Nor does the ideal tuning overly determine the choice of thermal mass material. As the performance data in Figure 13 show, concrete outperforms hardwood thermally—but surprisingly not by very much. (The hardwood

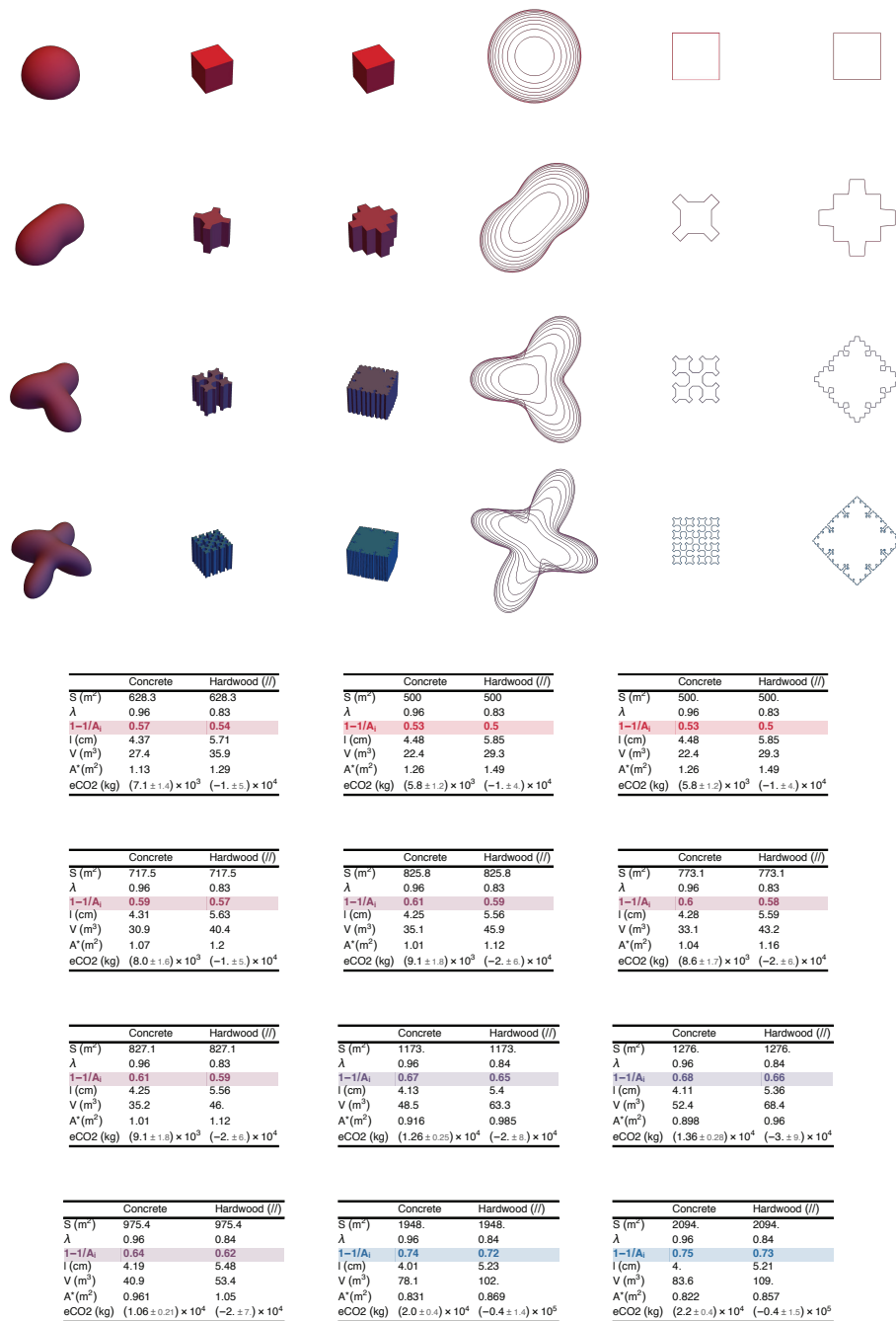


Figure 13: Blobs and castles. These optimized massings have different architectural styles, but all have height $H = 10$ m and ventilation enough for 100 people ($Q = 1 \text{ m}^3/\text{s}$). As the surface area increases, the floating interior temperature ($1-1/A_i$) cools, and the optimal thickness of thermal mass reduces. Concrete outperforms hardwood thermally, but surprisingly not by very much.

versions have slightly lower values for λ , hence $1 - 1/A_i$ is slightly reduced. The ventilation rate is maintained at $Q = 1 \text{ m}^3/\text{s}$ by slightly increasing A^*)

Notice how the morphologies in figure 13 have very different spatial qualities—from wings, courtyard niches, to open plans—which would have very different consequences for the inter-subjective experience of occupants. This simple example is enough to show how working with the ideal massing ratios (F/λ , Ω) can profoundly but playfully shape the development of an architectural concept from *part to whole*, from the type and thickness of the massing material to the spatial organization of the building.

5. Conclusion

§1 outlined the need for a new approach to building design in the early stages, which allows teams to evaluate the environmental impacts of primary material choices while showing them how to integrate as many functions into these primary materials as possible, so there is less need for other materials, products, and technologies, shrinking the ecological footprint. Shaping one material to integrate structure, thermal mass, and buoyancy ventilation, is a prominent place to start.

§2 showed that, while there has been lots of progress on efficient methods for simulating the effects of thermal mass in arbitrary configurations, none of this knowledge has been integrated and distilled into a workable set of parameters, to help architects and planners proportion thermal mass buildings properly, particularly in light of the challenges posed by climate change. The work by Holford and Woods [82]—who succinctly and accurately parameterized the coupling between thermal mass and buoyancy ventilation—was identified as the most promising basis for the much-needed design guidance.

Using these parametric definitions, the analysis in §3 found a new way to optimally synchronize the coupling of internal thermal mass and buoyancy ventilation. There is a choice between two damping coefficients to optimize for: the *peak venting temperature difference* or *attenuating temperature difference*. The performance of the building is then defined by relationship between two thermal parameters: F/λ (the ratio of ventilation heat transfer to surface heat transfer) and Ω (the ratio of thermal storage to surface heat transfer). When converted into optimal values, these parameters represent ideal ratios for tuning the form and mass of the building. Design teams then have the ability to synchronize ambient heat exchanges for their building in free-running mode, to meet chosen targets for the interior temperature and ventilation rate.

§4 demonstrated how to take these ideal ratios (F/λ , Ω) and materialize them into possible design options. One of the studies suggested that thin-shell structures of minimum weight, and even timber

buildings, may be optimally tuned to produce ample ventilation and temperature attenuation (c.f. §4.1). Another study showed how to break convention and fix the amount of material *before* design, as a way to respond to carbon caps becoming better defined and more stringent (c.f. §4.2). Another study showed how working with these ideal ratios (F/λ , Ω) could profoundly but playfully shape the development of an architectural concept from part to whole, including the spatial organization of the building, which determines the possible social interactions (c.f. §4.3).

Here is a summary of one possible calculation flow, as presented in §3 and §4. The design team decides on the free-running temperature (relative to the exterior swing of temperature), the rate of buoyancy ventilation (to satisfy the needs of occupants and their activities), the thermal massing material (which may serve a structural function, too), and the notional height of the building (which co-determines the potential energy for driving the buoyancy ventilation). The equations then give the optimum thickness and surface area of that material (operating as externally insulated thermal mass) and the necessary size of ventilation openings (i.e. the effective open area). The team can then evaluate a range of options that achieve the same performance but with different geometries and massing materials (and repeat the process with different inputs as necessary).

It is important to re-state the scope and limitations of this work. The method is meant to support concept generation and guide engineering studies towards convergence. It is tailored for strategic comparisons at the early stage of design, not absolute forecasts at the later stages of design (c.f. §1.3). The value for the heat transfer coefficient must be chosen carefully to fairly represent surface heat transfer (c.f. §3.2) and serve as a suitable proxy for average internal loads (c.f. §3.3). In a parametric study, a representative range of thermal property values should be used for each candidate material, to reflect the uncertain variation of these properties in the real world (c.f. §4.1). Once a configuration for the building is chosen, Equation (2.16) or Equation (2.17) should be solved to more accurately establish the free-running temperature and ventilation rate. Then further work is needed to test the detailed response in a range of scenarios (e.g. anharmonic loads from inside and outside) and to finalize the design (e.g. external insulation, windows, supplementary heating or cooling). As highlighted in §2.1 and §2.2, there are various methods available to more accurately model the physics once the design proposal is settled. One particularly important thing to analyze is how the balance of buoyancy forces, heat loads, and heat storage effects may play out over short and long time scales. Once these path-dependencies are understood, they can be strategically avoided or harnessed by design.

It is equally important to re-state the ambitions of this work. Researchers and new graduates are

invariably taken aback on their first exposure to the social dynamics of the industry (c.f. §1.2). In one way or another, the climate emergency will force the industry to build differently. True environmental advocates know that getting different stakeholders to converge on a suitable concept goes hand-in-hand with analyzing their feasibility. For radical integration to be a success—where intelligent configurations of primary materials replace add-on products and technologies, shrinking the ecological footprint—all contributors need to be on board. This kind of consensus implies a shared imagination of what is technically possible. Part of the role of research is to outline new ways of building to meet future challenges, even if these concepts challenge contemporary assumptions regarding comfort and desirability, and imply unconventional ways of inhabiting buildings.

References

[1] S. I. Seneviratne, M. G. Donat, A. J. Pitman, R. Knutti, R. L. Wilby, Allowable CO2 emissions based on regional and impact-related climate targets, *Nature* 529 (7587) (2016) 477–483. doi:10.1038/nature16542.

[2] C. A. Kennedy, I. Stewart, A. Facchini, I. Cersosimo, R. Mele, B. Chen, M. Uda, A. Kansal, A. Chiu, K. gon Kim, C. Dubeux, E. L. L. Rovere, B. Cunha, S. Pincetl, J. Keirstead, S. Barles, S. Pusaka, J. Gunawan, M. Adegbile, M. Nazariha, S. Hoque, P. J. Marcotullio, F. G. Otharán, T. Genena, N. Ibrahim, R. Farooqui, G. Cervantes, A. D. Sahin, Energy and material flows of megacities, *Proceedings of the National Academy of Sciences* 112 (19) (2015) 5985–5990. doi:10.1073/pnas.1504315112.

[3] J. M. Allwood, M. F. Ashby, T. G. Gutowski, E. Worrell, Material efficiency: providing material services with less material production, *Philosophical Transactions of the Royal Society of London A: Mathematical, Physical and Engineering Sciences* 371 (1986) (2013) 20120496. doi:10.1098/rsta.2012.0496.

[4] F. Pomponi, C. D. Wolf, A. Moncaster, *Embodied Carbon in Buildings: Measurement, Management, and Mitigation*, Springer, 2018.

[5] B. King, *The New Carbon Architecture: Building to Cool the Climate*, New Society Publishers, 2017.

[6] C. D. Wolf, F. Pomponi, A. Moncaster, Measuring embodied carbon dioxide equivalent of buildings: A review and critique of current industry practice, *Energy and Buildings* 140 (2017) 68–80. doi:10.1016/j.enbuild.2017.01.075.

[7] F. Pomponi, A. Moncaster, C. D. Wolf, Furthering embodied carbon assessment in practice: Results of an industry-academia collaborative research project, *Energy and Buildings* 167 (2018) 177–186. doi:10.1016/j.enbuild.2018.02.052.

[8] F. Pomponi, A. Moncaster, Briefing: BS 8001 and the built environment: a review and critique, *Proceedings of the Institution of Civil Engineers - Engineering Sustainability* 172 (3) (2018) 111–114. doi:10.1680/jensu.17.00067.

[9] A. M. Moncaster, F. Pomponi, K. E. Symons, P. M. Guthrie, Why method matters: Temporal, spatial and physical variations in LCA and their impact on choice of structural system, *Energy and Buildings* 173 (2018) 389–398. doi:10.1016/j.enbuild.2018.05.039.

[10] A. Dubois, L.-E. Gadde, The construction industry as a loosely coupled system: implications for productivity and innovation, *Construction Management and Economics* 20 (7) (2002) 621–631. doi:10.1080/01446190210163543.

- [11] M. F. Ashby, J. Fernandez, A. Gray, Unit 9. Architecture & Built Environment: Materials for Construction. Granta CES EduPack 2007 (2007).
- [12] B. D'Amico, F. Pomponi, A compactness measure of sustainable building forms, Royal Society Open Science 6 (6) (2019) 181265. doi:10.1098/rsos.181265.
- [13] M. J. Holmes, J. N. Hacker, Climate change, thermal comfort and energy: Meeting the design challenges of the 21st century, Energy and Buildings 39 (7) (2007) 802–814. doi:10.1016/j.enbuild.2007.02.009.
- [14] J. N. Hacker, T. P. D. Saulles, A. J. Minson, M. J. Holmes, Embodied and operational carbon dioxide emissions from housing: A case study on the effects of thermal mass and climate change, Energy and Buildings 40 (3) (2008) 375–384. doi:10.1016/j.enbuild.2007.03.005.
- [15] D. Fosas, D. A. Coley, S. Natarajan, M. Herrera, M. F. de Pando, A. Ramallo-Gonzalez, Mitigation versus adaptation: Does insulating dwellings increase overheating risk?, Building and Environment 143 (2018) 740–759. doi:10.1016/j.buildenv.2018.07.033.
- [16] W. H. Ko, S. Schiavon, G. Brager, B. Levitt, Ventilation, thermal and luminous autonomy metrics for an integrated design process, Building and Environment 145 (2018) 153–165. doi:10.1016/j.buildenv.2018.08.038.
- [17] H. Samuelson, S. Claussnitzer, A. Goyal, Y. Chen, A. Romo-Castillo, Parametric energy simulation in early design: High-rise residential buildings in urban contexts, Building and Environment 101 (2016) 19–31. doi:https://doi.org/10.1016/j.buildenv.2016.02.018.
- [18] D. Hawkes, The Environmental Imagination: Technics and Poetics of the Architectural Environment, Taylor & Francis Group, 2019.
- [19] M. H. Kurth, J. M. Keenan, M. Sasani, I. Linkov, Defining resilience for the US building industry, Building Research & Information 47 (4) (2019) 480–492. doi:10.1080/09613218.2018.1452489.
- [20] E. Shove, What is wrong with energy efficiency?, Building Research & Information 46 (7) (2018) 779–789. doi:10.1080/09613218.2017.1361746.
- [21] A. Baniassadi, J. Heusinger, D. J. Sailor, Energy efficiency vs resiliency to extreme heat and power outages: The role of evolving building energy codes, Building and Environment 139 (2018) 86–94. doi:https://doi.org/10.1016/j.buildenv.2018.05.024.
- [22] G. P. Henze, J. Pfaffert, S. Herkel, C. Felsmann, Impact of adaptive comfort criteria and heat waves on optimal building thermal mass control, Energy and Buildings 39 (2) (2007) 221–235. doi:10.1016/j.enbuild.2006.06.006.
- [23] K. J. Lomas, R. Giridharan, Thermal comfort standards, measured internal temperatures and thermal resilience to climate change of free-running buildings: A case-study of hospital wards, Building and Environment 55 (2012) 57–72. doi:10.1016/j.buildenv.2011.12.006.
- [24] S. Manu, Y. Shukla, R. Rawal, L. E. Thomas, R. de Dear, Field studies of thermal comfort across multiple climate zones for the subcontinent: India Model for Adaptive Comfort (IMAC), Building and Environment 98 (2016) 55–70. doi:https://doi.org/10.1016/j.buildenv.2015.12.019.
- [25] L. A. López-Pérez, J. J. Flores-Prieto, C. Ríos-Rojas, Adaptive thermal comfort model for educational buildings in a hot-humid climate, Building and Environment 150 (2019) 181–194. doi:https://doi.org/10.1016/j.buildenv.2018.12.011.
- [26] D. Coley, M. Herrera, D. Fosas, C. Liu, M. Vellei, Probabilistic adaptive thermal comfort for resilient design,

- Building and Environment 123 (2017) 109–118. doi:<https://doi.org/10.1016/j.buildenv.2017.06.050>.
- [27] M. Vellei, M. Herrera, D. Fosas, S. Natarajan, The influence of relative humidity on adaptive thermal comfort, Building and Environment 124 (2017) 171–185. doi:<https://doi.org/10.1016/j.buildenv.2017.08.005>.
- [28] E. Barbadilla-Martín, J. M. S. Lissén, J. G. Martín, P. Aparicio-Ruiz, L. Brotas, Field study on adaptive thermal comfort in mixed mode office buildings in southwestern area of Spain, Building and Environment 123 (2017) 163–175. doi:<https://doi.org/10.1016/j.buildenv.2017.06.042>.
- [29] S. Carlucci, L. Bai, R. de Dear, L. Yang, Review of adaptive thermal comfort models in built environmental regulatory documents, Building and Environment 137 (2018) 73–89. doi:<https://doi.org/10.1016/j.buildenv.2018.03.053>.
- [30] A. García, F. Olivieri, E. Larrumbide, P. Ávila, Thermal comfort assessment in naturally ventilated offices located in a cold tropical climate, Bogotá, Building and Environment 158 (2019) 237–247. doi:<https://doi.org/10.1016/j.buildenv.2019.05.013>.
- [31] R. de Dear, J. Kim, T. Parkinson, Residential adaptive comfort in a humid subtropical climate—Sydney Australia, Energy and Buildings 158 (2018) 1296–1305. doi:<https://doi.org/10.1016/j.enbuild.2017.11.028>.
- [32] Y. Song, Y. Sun, S. Luo, Z. Tian, J. Hou, J. Kim, T. Parkinson, R. de Dear, Residential adaptive comfort in a humid continental climate – Tianjin China, Energy and Buildings 170 (2018) 115–121. doi:<https://doi.org/10.1016/j.enbuild.2018.03.083>.
- [33] D. Sánchez-García, C. Rubio-Bellido, J. J. M. del Río, A. Pérez-Fargallo, Towards the quantification of energy demand and consumption through the adaptive comfort approach in mixed mode office buildings considering climate change, Energy and Buildings 187 (2019) 173–185. doi:<https://doi.org/10.1016/j.enbuild.2019.02.002>.
- [34] E. Barbadilla-Martín, J. G. Martín, J. M. S. Lissén, J. S. Ramos, S. Álvarez Domínguez, Assessment of thermal comfort and energy savings in a field study on adaptive comfort with application for mixed mode offices, Energy and Buildings 167 (2018) 281–289. doi:<https://doi.org/10.1016/j.enbuild.2018.02.033>.
- [35] A. Pérez-Fargallo, J. A. Pulido-Arcas, C. Rubio-Bellido, M. Trebilcock, B. Piderit, S. Attia, Development of a new adaptive comfort model for low income housing in the central-south of chile, Energy and Buildings 178 (2018) 94–106. doi:<https://doi.org/10.1016/j.enbuild.2018.08.030>.
- [36] Y. Chen, Z. Tong, A. Malkawi, Investigating natural ventilation potentials across the globe: Regional and climatic variations, Building and Environment 122 (2017) 386–396. doi:<https://doi.org/10.1016/j.buildenv.2017.06.026>.
- [37] E.-S. Im, J. S. Pal, E. A. B. Eltahir, Deadly heat waves projected in the densely populated agricultural regions of South Asia, Science Advances 3 (8) (2017) e1603322. doi:10.1126/sciadv.1603322.
- [38] S. Kang, E. A. B. Eltahir, North China Plain threatened by deadly heatwaves due to climate change and irrigation, Nature Communications 9 (1) (2018) 2894. doi:10.1038/s41467-018-05252-y.
- [39] Q. Schiermeier, Climate change made Europe’s mega-heatwave five times more likely, Nature (July 2019).
- [40] C. Ghiaus, Equivalence between the load curve and the free-running temperature in energy estimating methods, Energy and Buildings 38 (5) (2006) 429–435. doi:<https://doi.org/10.1016/j.enbuild.2005.08.003>.
- [41] C. Inard, J. Pfafferoth, C. Ghiaus, Free-running temperature and potential for free cooling by ventilation: A case study, Energy and Buildings 43 (10) (2011) 2705–2711. doi:<https://doi.org/10.1016/j.enbuild.2011.06.017>.
- [42] S. C. Sherwood, M. Huber, An adaptability limit to climate change due to heat stress, Proceedings of the National Academy of Sciences 107 (21) (2010) 9552–9555. doi:10.1073/pnas.0913352107.

- [43] J. S. Pal, E. A. B. Eltahir, Future temperature in southwest Asia projected to exceed a threshold for human adaptability, *Nature Climate Change* 6 (2) (2016) 197–200. doi:10.1038/nclimate2833.
- [44] J. D. Balcomb, Passive solar research and practice, *Energy and Buildings* 7 (4) (1984) 281–295. doi:10.1016/0378-7788(84)90074-4.
- [45] E. Krüger, E. G. Cruz, B. Givoni, Effectiveness of indirect evaporative cooling and thermal mass in a hot arid climate, *Building and Environment* 45 (6) (2010) 1422–1433. doi:10.1016/j.buildenv.2009.12.005.
- [46] S. Verbeke, A. Audenaert, Thermal inertia in buildings: A review of impacts across climate and building use, *Renewable and Sustainable Energy Reviews* 82 (2018) 2300–2318. doi:10.1016/j.rser.2017.08.083.
- [47] L. Yang, Y. Li, Cooling load reduction by using thermal mass and night ventilation, *Energy and Buildings* 40 (11) (2008) 2052–2058. doi:10.1016/j.enbuild.2008.05.014.
- [48] D. G. L. Samuel, S. M. S. Nagendra, M. P. Maiya, Passive alternatives to mechanical air conditioning of building: A review, *Building and Environment* 66 (2013) 54–64. doi:10.1016/j.buildenv.2013.04.016.
- [49] G. Reynders, T. Nuytten, D. Saelens, Potential of structural thermal mass for demand-side management in dwellings, *Building and Environment* 64 (2013) 187–199. doi:10.1016/j.buildenv.2013.03.010.
- [50] P. F. Linden, G. F. Lane-Serff, D. A. Smeed, Emptying filling boxes: The fluid mechanics of natural ventilation, *Journal of Fluid Mechanics* 212 (1990) 309–335. doi:10.1017/S0022112090001987.
- [51] P. F. Linden, The Fluid Mechanics of Natural Ventilation, *Annual Review of Fluid Mechanics* 31 (1) (1999) 201–238. doi:10.1146/annurev.fluid.31.1.201.
- [52] A. Acred, Natural ventilation in multi-storey buildings: a preliminary design approach (September 2014).
- [53] A. W. Woods, S. Fitzgerald, S. Livermore, A comparison of winter pre-heating requirements for natural displacement and natural mixing ventilation, *Energy and Buildings* 41 (12) (2009) 1306–1312. doi:10.1016/j.enbuild.2009.07.030.
- [54] A. S. Kuesters, A. W. Woods, A comparison of winter heating demand using a distributed and a point source of heating with mixing ventilation, *Energy and Buildings* 55 (2012) 332–340. doi:10.1016/j.enbuild.2012.07.045.
- [55] A. Acred, G. R. Hunt, A simplified mathematical approach for modelling stack ventilation in multi-compartment buildings, *Building and Environment* 71 (2014) 121–130. doi:10.1016/j.buildenv.2013.09.004.
- [56] A. Acred, G. R. Hunt, Stack ventilation in multi-storey atrium buildings: A dimensionless design approach, *Building and Environment* 72 (2014) 44–52. doi:10.1016/j.buildenv.2013.10.007.
- [57] S. A. Gage, G. R. Hunt, P. F. Linden, Top down ventilation and cooling, *Journal of Architectural and Planning Research* 18 (4) (2001) 286–301.
- [58] T. Chenvidyakarn, A. Woods, Top-down precooled natural ventilation, *Building Services Engineering Research and Technology* 26 (3) (2005) 181–193. doi:10.1191/0143624405bt129oa.
- [59] T. Chenvidyakarn, A. Woods, Stratification and oscillations produced by pre-cooling during transient natural ventilation, *Building and Environment* 42 (1) (2007) 99–112. doi:10.1016/j.buildenv.2005.08.007.
- [60] S. R. Livermore, A. W. Woods, On the effect of distributed cooling in natural ventilation, *Journal of Fluid Mechanics* 600 (2008) 1–17. doi:10.1017/S0022112007009809.
- [61] S. Sloman, P. Fernbach, *The Knowledge Illusion: Why We Never Think Alone*, Penguin, 2017.
- [62] H. King, S. Ocko, L. Mahadevan, Termite mounds harness diurnal temperature oscillations for ventilation, *Pro-*

- ceedings of the National Academy of Sciences 112 (37) (2015) 11589–11593. doi:10.1073/pnas.1423242112.
- [63] S. A. Ocko, H. King, D. Andreen, P. Bardunias, J. S. Turner, R. Soar, L. Mahadevan, Solar-powered ventilation of African termite mounds, *Journal of Experimental Biology* 220 (18) (2017) 3260–3269. doi:10.1242/jeb.160895.
- [64] S. Craig, Termite mound climate control (Dec 2017).
URL <https://massivesci.com/articles/termite-mound-arcology-climate-control/>
- [65] S. A. Ocko, A. Heyde, L. Mahadevan, Morphogenesis of termite mounds, *Proceedings of the National Academy of Sciences* 116 (9) (2019) 3379–3384. doi:10.1073/pnas.1818759116.
- [66] *Passive Solar Buildings*, MIT Press, 1992.
- [67] J. Fourier, *Theorie analytique de la chaleur*, par M. Fourier, chez Firmin Didot, pere et fils, 1822.
- [68] I. Stewart, *Seventeen Equations that Changed the World*, Profile Books, 2012.
- [69] P. Gruber, J. Toedtli, On the optimal thermal storage capability of a homogeneous wall under sinusoidal excitations, *Energy and Buildings* 13 (3) (1989) 177–186. doi:10.1016/0378-7788(89)90031-5.
- [70] P. Ma, L. S. Wang, Effective heat capacity of interior planar thermal mass (iPTM) subject to periodic heating and cooling, *Energy and Buildings* 47 (2012) 44–52. doi:10.1016/j.enbuild.2011.11.020.
- [71] *EnergyPlus Energy Simulation Software – EnergyPlus Documentation*, USA, Department of Energy, 2019.
URL <https://energyplus.net/documentation>
- [72] J. Clarke, *Energy Simulation in Building Design*, Routledge, 2007.
- [73] C. Underwood, F. Yik, *Modelling Methods for Energy in Buildings*, John Wiley & Sons, 2008.
- [74] A. Athienitis, W. O'Brien, *Modeling, Design, and Optimization of Net-Zero Energy Buildings*, John Wiley & Sons, 2015.
- [75] J. Hillary, E. Walsh, A. Shah, R. Zhou, P. Walsh, Guidelines for developing efficient thermal conduction and storage models within building energy simulations, *Energy* 125 (2017) 211–222. doi:10.1016/j.energy.2017.02.127.
- [76] J. Hillary, E. Walsh, A. Shah, R. Zhou, P. Walsh, Universal approach to modelling multi-layer structures in building energy simulations, *Energy and Buildings* 170 (2018) 122–133. doi:10.1016/j.enbuild.2018.04.009.
- [77] C. P. Underwood, An improved lumped parameter method for building thermal modelling, *Energy and Buildings* 79 (2014) 191–201. doi:10.1016/j.enbuild.2014.05.001.
- [78] R. Cheng, X. Wang, Y. Zhang, Analytical optimization of the transient thermal performance of building wall by using thermal impedance based on thermal-electric analogy, *Energy and Buildings* 80 (2014) 598–612. doi:10.1016/j.enbuild.2014.05.023.
- [79] *ApacheSim Calculation Methods*, Integrated Environmental Solutions Ltd., Glasgow, 2019 (2019).
URL <http://www.iesve.com/downloads/help/Thermal/Reference/ApacheSimCalculationMethods.pdf>
- [80] E. Mantesi, C. J. Hopfe, M. J. Cook, J. Glass, P. Strachan, The modelling gap: Quantifying the discrepancy in the representation of thermal mass in building simulation, *Building and Environment* 131 (2018) 74–98. doi:10.1016/j.buildenv.2017.12.017.
- [81] J. Yam, Y. Li, Z. Zheng, Nonlinear coupling between thermal mass and natural ventilation in buildings, *International Journal of Heat and Mass Transfer* 46 (7) (2003) 1251–1264. doi:10.1016/S0017-9310(02)00379-4.
- [82] J. M. Holford, A. W. Woods, On the thermal buffering of naturally ventilated buildings through internal thermal mass, *Journal of Fluid Mechanics* 580 (2007) 3–29. doi:10.1017/S0022112007005320.

- [83] J. Zhou, G. Zhang, Y. Lin, Y. Li, Coupling of thermal mass and natural ventilation in buildings, *Energy and Buildings* 40 (6) (2008) 979–986. doi:10.1016/j.enbuild.2007.08.001.
- [84] J. Zhou, G. Zhang, Y. Lin, H. Wang, A new virtual sphere method for estimating the role of thermal mass in natural ventilated buildings, *Energy and Buildings* 43 (1) (2011) 75–81. doi:10.1016/j.enbuild.2010.08.015.
- [85] B. Lishman, A. W. Woods, The effect of gradual changes in wind speed or heat load on natural ventilation in a thermally massive building, *Building and Environment* 44 (4) (2009) 762–772. doi:10.1016/j.buildenv.2008.06.026.
- [86] T. Chenvidyakarn, A. Woods, Multiple steady states in stack ventilation, *Building and Environment* 40 (3) (2005) 399–410. doi:10.1016/j.buildenv.2004.06.020.
- [87] J. Yuan, L. R. Glicksman, Multiple steady states in combined buoyancy and wind driven natural ventilation: The conditions for multiple solutions and the critical point for initial conditions, *Building and Environment* 43 (1) (2008) 62–69. doi:10.1016/j.buildenv.2006.11.035.
- [88] N. B. Kaye, Y. Ji, M. J. Cook, Numerical simulation of transient flow development in a naturally ventilated room, *Building and Environment* 44 (5) (2009) 889–897. doi:10.1016/j.buildenv.2008.06.016.
- [89] X. Faure, N. L. Roux, Time dependent flows in displacement ventilation considering the volume envelope heat transfers, *Building and Environment* 50 (2012) 221–230. doi:10.1016/j.buildenv.2011.11.007.
- [90] T. Chenvidyakarn, *Buoyancy effects on natural ventilation*, Cambridge University Press, Cambridge ; New York, 2013.
- [91] D. Yang, Y. Guo, Fluctuation of natural ventilation induced by nonlinear coupling between buoyancy and thermal mass, *International Journal of Heat and Mass Transfer* 96 (2016) 218–230. doi:10.1016/j.ijheatmasstransfer.2016.01.017.
- [92] D. Bastien, A. K. Athienitis, Passive thermal energy storage, part 1: Design concepts and metrics, *Renewable Energy* 115 (2018) 1319–1327. doi:10.1016/j.renene.2016.04.011.
- [93] D. Bastien, A. K. Athienitis, Passive thermal energy storage, part 2: Design methodology for solar and greenhouses, *Renewable Energy* 103 (2017) 537–560. doi:10.1016/j.renene.2016.11.041.
- [94] B. M. Jones, M. J. Cook, S. D. Fitzgerald, C. R. Iddon, A review of ventilation opening area terminology, *Energy and Buildings* 118 (2016) 249–258. doi:10.1016/j.enbuild.2016.02.053.
- [95] H. B. Awbi, A. Hatton, Mixed convection from heated room surfaces, *Energy and Buildings* 32 (2) (2000) 153–166. doi:10.1016/S0098-8472(99)00063-5.
- [96] H. B. Awbi, Calculation of convective heat transfer coefficients of room surfaces for natural convection, *Energy and Buildings* 28 (2) (1998) 219–227. doi:10.1016/S0378-7788(98)00022-X.
- [97] A. Novoselac, B. J. Burley, J. Srebric, New Convection Correlations for Cooled Ceiling Panels in Room with Mixed and Stratified Airflow, *HVAC&R Research* 12 (2) (2006) 279–294. doi:10.1080/10789669.2006.10391179.
- [98] M. A. Menchaca-Brandan, F. A. D. Espinosa, L. R. Glicksman, The influence of radiation heat transfer on the prediction of air flows in rooms under natural ventilation, *Energy and Buildings* 138 (2017) 530–538. doi:10.1016/j.enbuild.2016.12.037.
- [99] *Handbook of heat transfer*, McGraw-Hill, 1998.
- [100] G. Nellis, S. A. Klein, *Heat transfer*, Cambridge University Press, Cambridge; New York, 2009.
- [101] M. F. Ashby, *Materials and the environment : eco-informed material choice*, 2nd Edition, Elsevier/Butterworth-

Heinemann, Amsterdam ; Boston, 2013.

[102] C. D. Perna, F. Stazi, A. U. Casalena, M. D'Orazio, Influence of the internal inertia of the building envelope on summertime comfort in buildings with high internal heat loads, *Energy and Buildings* 43 (1) (2011) 200–206. doi:10.1016/j.enbuild.2010.09.007.

[103] H. Wang, Q. Chen, A semi-empirical model for studying the impact of thermal mass and cost-return analysis on mixed-mode ventilation in office buildings, *Energy and Buildings* 67 (2013) 267–274. doi:10.1016/j.enbuild.2013.08.025.

[104] T. Wangler, N. Roussel, F. P. Bos, T. A. M. Salet, R. J. Flatt, Digital Concrete: A Review, *Cement and Concrete Research* 123 (2019) 105780. doi:10.1016/j.cemconres.2019.105780.

[105] M. Popescu, L. Reiter, A. Liew, T. V. Mele, R. J. Flatt, P. Block, Building in Concrete with an Ultra-lightweight Knitted Stay-in-place Formwork: Prototype of a Concrete Shell Bridge, *Structures* 14 (2018) 322–332. doi:10.1016/j.istruc.2018.03.001.

[106] R. A. Buswell, W. R. L. de Silva, S. Z. Jones, J. Dirrenberger, 3D printing using concrete extrusion: A roadmap for research, *Cement and Concrete Research* 112 (2018) 37–49. doi:10.1016/j.cemconres.2018.05.006.

[107] S. J. Keating, J. C. Leland, L. Cai, N. Oxman, Toward site-specific and self-sufficient robotic fabrication on architectural scales, *Science Robotics* 2 (5) (2017) eaam8986. doi:10.1126/scirobotics.aam8986.

[108] M. West, *The Fabric Formwork Book: Methods for Building New Architectural and Structural Forms in Concrete*, Routledge, 2016.

[109] S. Adriaenssens, P. Block, D. Veenendaal, C. Williams, *Shell Structures for Architecture: Form Finding and Optimization*, Routledge, 2014.

[110] D. Veenendaal, M. West, P. Block, History and overview of fabric formwork: using fabrics for concrete casting, *Structural Concrete* 12 (3) (2011) 164–177. doi:10.1002/suco.201100014.

[111] J.-F. Bastin, Y. Finegold, C. Garcia, D. Mollicone, M. Rezende, D. Routh, C. M. Zohner, T. W. Crowther, The global tree restoration potential, *Science* 365 (6448) (2019) 76–79. doi:10.1126/science.aax0848.

[112] B. King, *The New Carbon Architecture: Building to Cool the Climate*, New Society Publishers, 2017.

[113] D. Wood, C. Vailati, A. Menges, M. Rüggeberg, Hygroscopically actuated wood elements for weather responsive and self-forming building parts – Facilitating upscaling and complex shape changes, *Construction and Building Materials* 165 (2018) 782–791. doi:10.1016/j.conbuildmat.2017.12.134.

[114] *Advancing Wood Architecture: A Computational Approach*, 1st Edition, Routledge, London ; New York, 2016.

[115] A. Laborel-Préneron, C. Magniont, J.-E. Aubert, Hygrothermal properties of unfired earth bricks: Effect of barley straw, hemp shiv and corn cob addition, *Energy and Buildings* 178 (2018) 265–278. doi:10.1016/j.enbuild.2018.08.021.

[116] D. U. Shah, M. C. D. Bock, H. Mulligan, M. H. Ramage, Thermal conductivity of engineered bamboo composites, *Journal of Materials Science* 51 (6) (2016) 2991–3002. doi:10.1007/s10853-015-9610-z.

[117] E. W. Weisstein, Legendre Polynomial.

URL <http://mathworld.wolfram.com/LegendrePolynomial.html>

[118] E. W. Weisstein, Sierpiński Curve.

URL <http://mathworld.wolfram.com/SierpinskiCurve.html>

- 1019 [119] E. W. Weisstein, Cesàro Fractal.
1020 URL <http://mathworld.wolfram.com/CesaroFractal.html>
1021 [120] E. W. Weisstein, Koch Snowflake.
1022 URL <http://mathworld.wolfram.com/KochSnowflake.html>